# Growth, characterization and device fabrication of two dimensional materials


**Kumar Priyadarshi**

**20121015**

**Final year project in Physics**

**In Partial Fulfilment of the Requirements for BS MS Dual Degree programme**


**Department of Physics**

**Indian institute of Science Education & Research, Pune.**


**AY 2016/17**

# Declaration

I, hereby declare that the matter embodied in the report entitled "**Growth, characterization and device fabrication of two dimensional materials**" are the results of the work carried out by me at the Department of Materials Processing and Characterization and Department of Ceramics at **Institute of Materials Research and Engineering (IMRE)** under the supervision of **Dr. Swee Liang Wong** and the same has not been submitted elsewhere for any other degree.

Dr. ~~Wong~~ Swee Liang Wong
Scientist I
IMRE, Singapore.

Kumar Priyadarshi
20121015
BS MS 5th year

Scanned by CamScanner

## Certificate

This is to certify that this dissertation entitled "**Growth, characterization and device fabrication of two dimensional materials**" towards the partial fulfillment of the BS-MS dual degree programme at the Indian Institute of Science Education and Research, Pune represents study/work carried out by **Kumar Priyadarshi** at **Institute of Materials Research and Engineering (IMRE) and National University of Singapore** under the supervision of **Dr. Swee Liang Wong,** Scientist I, IMRE during the academic year **2016-17.**

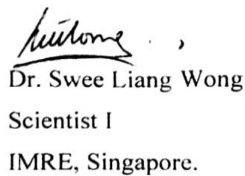

Dr. Swee Liang Wong

Scientist I

IMRE, Singapore.

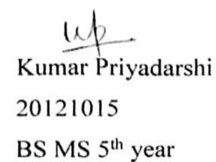

Kumar Priyadarshi

20121015

BS MS 5th year

Scanned by CamScanner

## Acknowledgement

First and foremost, I would like to express my deepest gratitude towards my supervisors Dr Wong Swee Liang and Prof. Andrew Wee. Their patient guidance and advice has proved invaluable; without which it would not be possible for me to acquire the necessary skills to bring this project to a desired completion. In spite of having a full workload, their meticulous and tireless review of my manuscripts and experimental work, as well as expressing such care and concern for their students has made an impression on me regarding the immense dedication and professionalism they take towards research.

I would like to give my special thanks to Dr Wong Swee Liang for his constructive suggestions and support by means of spending much time and effort in addressing my questions and doubts. He selflessly taught me experimental techniques, literature and most importantly research methodology which will be useful for me in all the future research ventures.

I also want to express a sincere thanks to Dr. Aparna Deshpande, IISER Pune for her constant guidance and support during last few months. She has given inputs and suggestions to improve the work that I am doing. The successful completion of this project would not have been possible without her motivation and guardianship.

I am also thankful to Shashank Srivastava for teaching me software to make schematic, Deepshikha Arora for reading and providing inputs for the thesis report, Kishor Bharti for teaching me Latec, Sai Balaji and Vignesh Raman for their constant support over the last few months. Their kind camaraderie and support provided is priceless and will be highly cherished.

Finally, I am also grateful for the love and support that my family has shown me over this period. Their support has constantly spurred me to greater heights.

**Table of Contents**


Front page………………………………………………………………… 1

Certificate………..……………………………………………………… 2

Declaration……...………………………………………………………… 3

Acknowledgement………………………………………………………… 4

Table of Contents..……………………………………………………… 5

List of Figures…………………………………………………………… 6-7

List of Tables……………………………………………………………. 8

Summary…………………………………………………………………. 9

**Chapter 1: Introduction**………………………………………………. 7

1.1 Properties and Applications of TMDCs……………………………….. 8

1.2 Synthesis ………………………………………………………………. 12

1.2.1: Chemical Vapour Deposition……………………………………… 13

1.3 Characterization………………………………………………………… 17

1.4: Field Effect transistors…………………………………………………. 20

**Chapter 2: Experimental Methods**……………………………………… 21

2.1 Conventional Growth…………………………………………………… 21

2.2 Proposed new method…………………………………………………… 23

2.3 Device Fabrication……………………………………………………… 25

**Chapter 3: Results and Discussion** ………………………………………… 26

3.1: Optical Characterization………………………………………………… 26

3.1.1: Conventional Growth…………………………………………………… 26

31.2: Proposed new method………………………………………………… 29

3.2: Raman and PL mapping………………………………………………… 31

3.3 Atomic Force Microscopy……………………………………………… 33

3.3 X-ray Photoelectron Spectroscopy……………………………………… 34

3.4 Transport measurements………………………………………………… 38

3.5: Advantages of proposed method………………………………………… 39

**Chapter 4: Conclusion and Outlook**………………………………………… 40

4.1 Thesis Summary ........................................................................................ 40

4.2 Future Work ........................................................................................... 40

**References** …………………………………………………………………… 43-44

**List of Figures: Parenthesis shows the page number for the figure**

**Fig. 1**: Family of 2D materials. {9}

**Fig. 2**: Structure of monolayer TMDC.{10}

**Fig. 3**: Atomic configurations of different TMD phases {12}

**Fig. 4**: Band Structure of $MoS_2$ {13}

**Fig. 5**: Basic CVD growth process {16}

**Fig. 6**: Different setup of CVD growth {17}

**Fig. 7**: CVD growth mechanism {17, 18}

**Fig. 8**: Schematic of an n-type MOSFET {21}

**Fig. 9**: Possible FET configurations {22}

**Fig. 10**: Conventional CVD setup to grow $MoS_2$ {25}

**Fig. 11**: Phase diagram for the possible pathways to produce $MoS_2$. {25}

**Fig. 12**: Proposed new setup geometry {24}

**Fig. 13**: Temperature Vs Time curve for different steps of the reaction {25}

**Fig. 14**: Optical image of Top-gate FET fabricated on $MoS_2$ single layers {26}

**Fig. 15**: Optical Images of monolayer $MoS_2$ at various temperatures {27}

**Fig. 16**: Comparison of Raman Peaks of $MoS_2$ at different temperatures. {28}

**Fig. 17**: Comparison of PL Peaks of $MoS_2$ at different temperatures. {28}

**Fig. 18**: Camera image of $MoS_2$ grown on sapphire using conventional setup {29}

**Fig. 19**: Camera image of $MoS_2$ grown on cm scale sapphire using proposed method {30}

**Fig. 20**: Optical microscope images of mm scale continuous layers and single layer triangles. {31}

**Fig. 21**: Raman peak separation of two modes {31}

**Fig. 22**: PL peaks at 1.9 eV confirms the formation of single layers. {32}

**Fig. 23**: Raman and PL mapping of $MoS_2$ monolayers {33}

**Fig. 24**: AFM images recorded from epi-ready c-plane sapphire wafers {34}

**Fig. 25**: AFM image of $MoS_2$ triangle formed. {35}

**Fig. 26**: Height profile of single layer {35}

**Fig. 27**: XPS Spectra of Mo 3d peak {36}

**Fig. 28**: Survey on $MoS_2$ thin films showing absence of Ni peak {36}

**Fig. 29:** Drain Current ($I_d$) Vs. Drain voltage ($V_D$) of device before anneal {37}

**Fig. 30:** Drain Current ($I_d$) Vs. Drain voltage ($V_D$) after anneal {38}

**Fig. 31:** Drain Current ($I_D$) Vs. Gate voltage ($V_G$) after anneal {38}

**Fig. 32:** $MoS_2$ monolayer triangles grown on a TEM grid using proposed method.{39}

**Fig. 33:** TEM image of $MoS_2$ crystals {40}

**List of Tables:**

**Table 1:** Summary of commonly used characterization techniques {19}

**Table 2:** Summary of reaction temperature optimization for conventional setup {29}

# ABSTRACT

In this thesis, a new method to grow large area monolayer $MoS_2$ on sapphire using Chemical Vapour Deposition (CVD) has been devised and demonstrated. An extensive and detailed analysis of growth mechanism was done. Raman, photoluminescence (PL) spectroscopy were used to confirm the monolayers as seen from optical microscope. Top gated field effect transistors (FETs) were fabricated to do the electrical characterization and transport measurements.

At first, the conventional method was optimized on the system as a reference point for the proposed growth method. Taking the associated growth parameters as the basis, a new CVD growth method was implemented. Once optimized, the new method produces single layer $MoS_2$ monolayers in the order of hundred microns and continuous $MoS_2$ single layers of centimetre scale. Optical characterization was done using optical microscope, Raman and PL spectroscopy. Raman and PL mapping were also done to check the homogeneity of layers formed. The height profile analysis was done using atomic force microscopy(AFM). X-ray photoelectron spectroscopy (XPS) was used to analyse elemental compositions and to quantize the impurities resulting from the new growth method.

In addition, top gated FET was fabricated and the electronic quality of the films was investigated through their associated transfer characteristics.

# Chapter I: INTRODUCTION

Layered materials have been studied for more than a century, but only after the seminal work on Graphene in 2004 [1], the realization of the vast potential of these materials seem possible. Decades before the mechanical exfoliation of Graphene, Frindt et al. [2] shown that van der Waals materials such as Transition Metal Dichalcogenides (TMDCs) could be thinned down into single layers using mechanical and chemical methods. Although the early work by Frind focused on obtaining and characterizing these layers, the unique properties exhibited by these materials were not explored. The Noble prize winning work on Graphene has triggered much research interest not only in graphene, but also has opened a new area of research in other 2D materials such as boron nitride (BN) and TMDCs having unique physical properties, which are not present in their 3D counterpart [3].

The recent surge of intensive research on these materials has opened a new sub category of "Fermi-Dirac" physics [4, 5]. Intensive efforts from both industry and academia in two-dimensional(2D) materials research have shown that bulk 3D counterparts of these materials, once thinned down to a monolayer show diverse electronic [4], optical [3] properties and have high surface to volume ratio that are absent in their 3D form.

Although 2D material research is only a decade old, it has already blossomed into a field of exciting possibilities ranging from fundamental physics to industrial applications. Many synthesis, transfer, detection, characterization of layered materials have been shown. Applications ranging from electronics to optoelectronics, biosensors to thermal conductors have been explored. Novel synthetic methods including top down and bottom up approaches have provided routes to exfoliate or grow new single- materials which is single atom thick. These synthetic routes have enabled the field of 2D materials to progress quite rapidly. An entire periodic table of atomically thin 2D materials [6] has emerged post graphene, (Fig. 1) having different physical properties and can be used in different applications.

Graphene, because of a zero band gap, is difficult to be used in digital electronic devices which require sufficient on-off ratios, despite having a huge mobility compared to all materials that are currently in use. It can still be used as electrodes. TMDCs have

also attracted much attention due to the presence of a band gap, diverse chemistry and abundance in nature.

| Graphene family | Graphene | hBN 'white graphene' | BCN | Fluorographene | Graphene oxide |
|---|---|---|---|---|---|
| 2D chalcogenides | $MoS_2$, $WS_2$, $MoSe_2$, $WSe_2$ | Semiconducting dichalcogenides: $MoTe_2$, $WTe_2$, $ZrS_2$, $ZrSe_2$ and so on | Metallic dichalcogenides: $NbSe_2$, $NbS_2$, $TaS_2$, $TiS_2$, $NiSe_2$ and so on | Layered semiconductors: GaSe, GaTe, InSe, $Bi_2Se_3$ and so on | |
| 2D oxides | Micas, BSCCO | $MoO_3$, $WO_3$ | Perovskite-type: $LaNb_2O_7$, $(Ca,Sr)_2Nb_3O_{10}$, $Bi_4Ti_3O_{12}$, $Ca_2Ta_2TiO_{10}$ and so on | Hydroxides: $Ni(OH)_2$, $Eu(OH)_2$ and so on | |
| | Layered Cu oxides | $TiO_2$, $MnO_2$, $V_2O_5$, $TaO_3$, $RuO_2$ and so on | | Others | |

**Fig. 1:** Family of 2D materials. [6]

**1.1: Properties and Applications of TMDCS:**

Transition metal dichalcogenides (TMDCs), a special class of 2D materials, are transition metal atoms sandwiched between two layers of chalcogens. Single and few odd layer TMDCs have broken out of plane symmetry and in plane inversion symmetry with chemical formula $MX_2$, where M and X represent the central transition metal atom and the surrounding chalcogen atoms (Mo, S, Se) respectively, as shown in Fig. 2(a-e). Atoms of the same layer are covalently bonded in a hexagonal lattice while adjacent layers are held by weak van der Waals forces, allowing thinning of the stack to easily take place. $MoS_2$, $WS_2$, $WSe_2$ and $MoSe_2$ are some examples of TMDCs which are actively researched. Depending on the elements involved as well as the structural arrangement between different physical phases, their electronic properties will vary which allows flexibility in a wide range of applications. $MoS_2$, a member of TMDC family, is one of the most studied 2D materials after graphene. It is an intrinsically n doped semiconductor and has remarkable electronic properties. Several optical and transport characteristics of $MoS_2$ [4, 6-8] have been reported in single and few layer $MoS_2$ [9]. A direct gap in monolayer form with strong excitonic effects and the possibility of spintronics by optical pumping with circularly polarized light [10, 11] and FET with high current on off ratios are also shown for $MoS_2$. These properties suggest potential applications of this TMDC in electronics and optoelectronics.

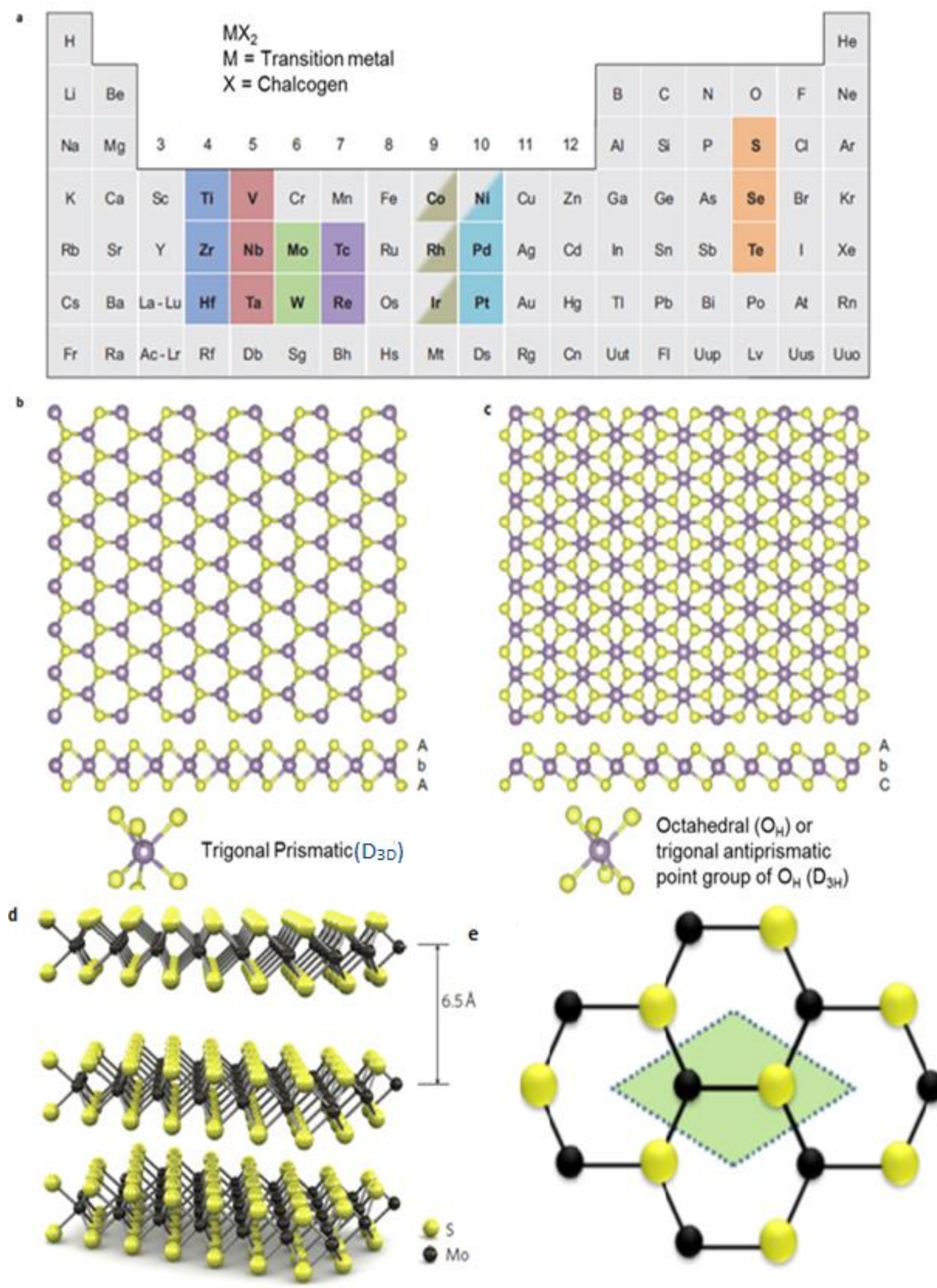


**Fig. 2:** Structure of monolayered TMDs. (a) Periodic table indicating the individual elements which can from TMDCs.(b) single-layer TMD with trigonal prismatic coordinations (c) single-layer TMD with octahedral coordinations. Here purple represents metal, yellow represents chalcogen and AbA and AbC represent the stacking sequence

where the upper- and lower-case letters represent chalcogen and metal elements, respectively. d) 3D representation of $MoS_2$ crystal structure showing the interlayer separation being 6.5 Å. e) honeycomb lattice structure in TMDCs, which shows the breaking of inversion symmetry. Panels a), b) and c) are taken from Ref. [15], Panel d) from Ref.[16] and Panel e) is from Ref. [17].

The few phases of $MoS_2$, which can be switched back and forth using electronic modification [13] or external strain [14] are 2H, 1T, 1T' and 1T". We can see that 1T phase can be derived from 2H phase from a structural transition where the S atoms on one side of the Mo atoms are shifted to coincide (in the top view) with the centres of the hexagons formed by Mo and S atoms resulting in a change of the symmetry from P63/mmc to P3.(Fig. 3a) The 1T' (Fig. 3b) and 1T" (Fig. 3c) phases transition can be induced by further distortions (from 1T phase) of the Mo chain.

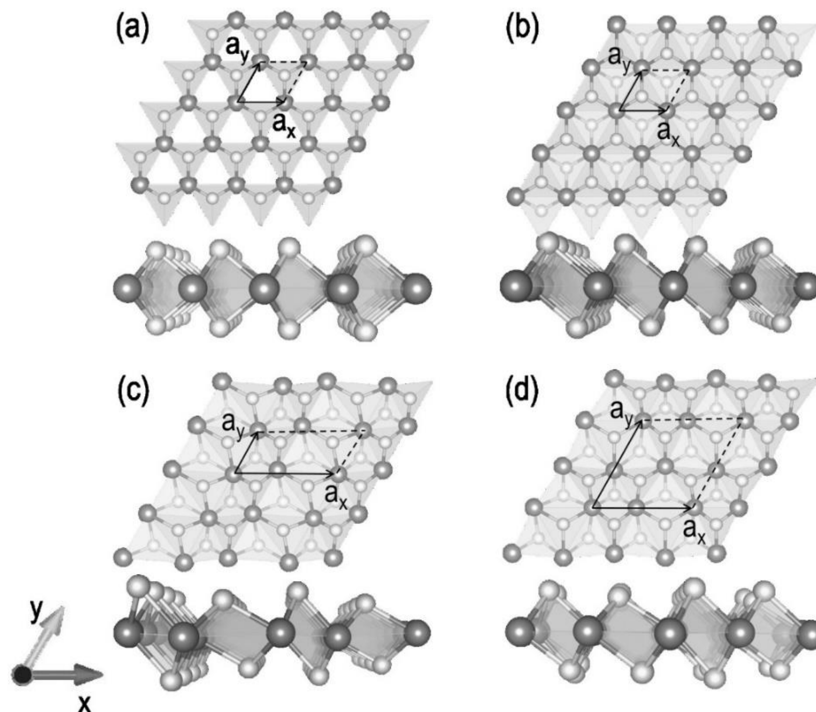


**Fig. 3**: Atomic configurations of different TMD phases: (a) 2H, (b) 1T, (c) 1T′, and (d) 1T″ phases. The black quadrilateral illustrates the unit cell, with the large dark and small bright spheres indicating metal and chalcogen atoms, respectively.[18]

$MoS_2$ monolayer has honeycomb lattice like graphene, the only difference being that A and B sub lattices are occupied either by Mo atoms or by a pair of S atoms rather than both being occupied by carbon atoms in graphene (Fig. 1). This slight difference in

the two sub lattices results in the opening of band gap by lifting the degeneracy in the electronic structure at the K point in first brillouin zone. This degeneracy in case of graphene is responsible for distinctive dirac cone dispersion relation in graphene [1]. MoS2 in bulk is an indirect band gap semiconductor which transforms to direct band gap semiconductor when thinned down to monolayer (Fig. 4). Similar changes in the electronic structures are reported for other semiconductor TMDCs [12] like $MoSe_2$.

2D materials, because of their electrostatic properties have an innate advantage over conventional materials in use like Silicon for device fabrication. Screening length(λ) for single and double gated geometry is given by [19]

$$\lambda = \sqrt{\frac{\in_s d_s d_{ox}}{\in_{ox}}} \qquad [1]$$

λ is screening length
and $\in_s$ is dielectric constant and $\in_{ox}$ is thickness of dielectric oxide.
$d_s$ is thickness of semiconductor and $d_{ox}$ is dielectric constant.

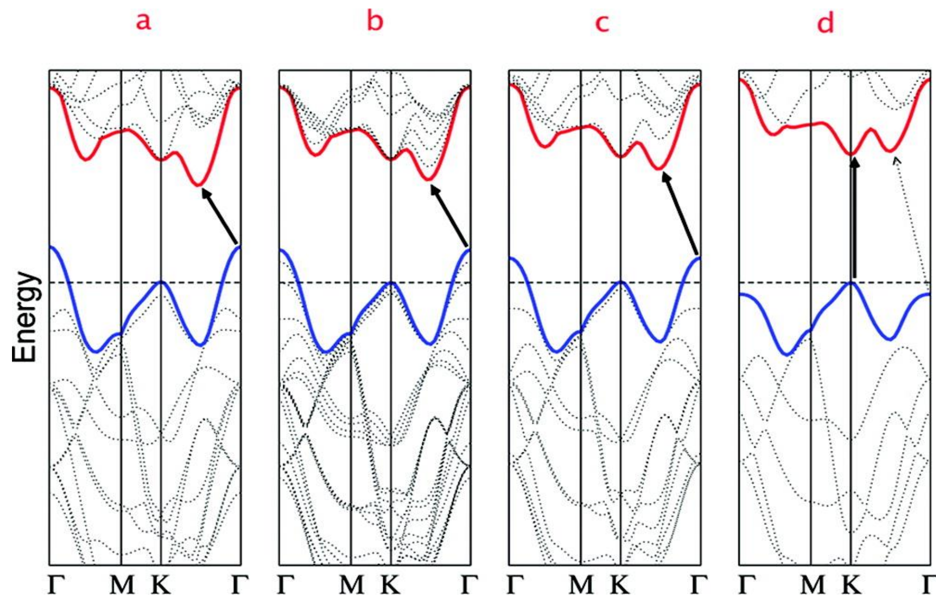


**Fig. 4**: Band Structures of (a) Bulk MoS2 where conduction band minima at different position in momentum space from that of valence band maxima suggesting indirect band gap (b) Quadrilayer $MoS_2$ depicting shift in conduction band minima towards valence band maxima (c) Bilayer MoS2 (d) Monolayer MoS2 where conduction band minima finally matches with valence band minima in momentum space suggesting the transition from indirect(1.9 eV) to direct band gap(1.2 eV) transition.[20]

As evident from equation 1, screening length (λ) is proportional to the thickness of semiconductor. Due to reduced dimensionality, these materials are a perfect candidate to approach ideal effective screening length λ (The criteria for minimum channel length L is 2 λ) and devices based on these can be operated beyond the quantum capacitance limit (QCL), a term related to the density of states. Quantum capacitance is important for systems with low density of states which is the case in a 2D electronic system in a semiconductor surface. In a parallel-plate capacitor, where density of states is uneven on two plates, the capacitance is not given by the general formula for parallel-plate capacitors. Capacitance decreases, as if the two capacitors are in series. This second capacitance which is a function of the density of states of the plates is called quantum capacitance.

To reduce the channel length, the semiconductor thickness must also be reduced to ensure that 2D electrostatic screening effects are minimized [21]. In a small channel, to make sure that drain's electric field does not get screened off completely as in case ultra-scaled MOSFETs, screening length should be as small as possible. From eqn. 1, $d_s$ should be minimized to make λ small. In the scenario explained, 2D material provides a very good alternative to silicon in device fabrication.

### 1.2 Synthesis :

2D TMDCs can be produced through both top-down and bottom-up methods. When 3D bulk counterpart is thinned down to its constituent layers using various means, it is called top-down approach and when single layers are grown from its constituents using chemical precursors, it is called bottom up approach. Mechanical, chemical and liquid exfoliation from bulk crystals is top down approaches. Mechanical exfoliation allows us to produce crystals which are of high-quality compared to other methods and are suitable for fundamental research and device fabrication. However, it is greatly limited by the randomness in thicknesses of the flakes that can be obtained as well as its low yield which prevents potential scaling up. Chemical exfoliation of monolayer TMDs is based on liquid-phase method, which provides useful films for printable electronics. However, the chemical method may result in altering the lattice structure of thin TMD layers or introduce impurities and thus require a treatment to regain the structure of monolayer TMDs. Scalability in large area and quality of films remains an issue in this method too.

For practical application of these materials in electronic and optical devices, large area synthesis of TMDCs with layer controlled and uniformity is an important requirement. As discussed above, mechanical and chemical exfoliation approach fails in the purpose. Chemical Vapour Deposition (CVD), a vapour phase based growth route is shown potential to produce TMDC monolayers with larger grain size, uniformity in layers and enhanced electronic properties in the last few years. [27,34] The obtained films have been successfully shown to be used in Nano electronics and for constructing layered 2D hetero structures. [4, 6] Due to the self-limiting nature of C atoms on the surface of metals such as Ni and Cu [22], growth of graphene on these substrates is easier rather the case of TMDCs, which does not have this property. This poses a challenge for controlling the growth dynamics and film deposition as per our requirement. [23] The quality of materials formed depends on the various growth conditions such as precursor concentration, placement of substrate w.r.t substrate, temperature, pressure, airflow. These parameters determine the lateral grain size and the layer thickness. [3]

**1.2.1: Chemical Vapour Deposition:**

CVD, a hybrid method to deposit gaseous reactants onto a substrate is used to grow 2D materials. With the possibility of depositing materials of a variety of chemical configurations, easy handling, and cheap and simple instrumentation allows CVD to be used for scientific as well as industrial purposes. Nano crystalline films or single crystalline films can also be grown using this method. [24]

The quality of deposited materials in CVD process is usually very high, making it a preferential growth method over other alternatives. CVD, being a relatively cheaper method, is also very popular growth route for industrial purposes and produces highly pure films. Diverse formats of CVD exist, but the most modern processes are categorized as per their associated operating pressure: LPCVD- Lower pressures chemical vapour deposition and UHVCVD- Ultra High Vacuum chemical vapour deposition. CVD procedure done under sub-atmospheric pressures is LPCVD. The low pressure has two major roles i.e. to avoid unwanted reactions and also producing uniform thickness of deposited material on the substrate. Exceptionally low atmospheric pressures are used for UHVCVD, usually in the region of $10^{-6}$ Pa. Other variants of CVD include MOCVD- Metallic Organic CVD, ALE- Atomic Layer Epitaxy, VPE- Vapour Phase Epitaxy, and PECVD- Plasma Enhanced CVD. They differ in source gas pressure, geometrical layout and temperature used. [24][1]

CVD process involves gaseous or vapour reactants to be transported towards the substrate (Fig. 5) in a reaction chamber using carrier gases such as $N_2$/ $H_2$/ Ar. The tube is typically set at ambient temperature. The substrate is kept at higher temperatures where the reactants break into various products and start to diffuse on the surface. When the combined gases meet the substrate within the heated reaction chamber, reaction occurs and precursors form intermediate particles which in turn form the desired material film on surface of substrate by nucleation and growth. The temperature of the substrate is one parameter which describes the type of reaction which will occur, so optimization of temperature is highly crucial. [24]

Parameters which govern rate of growth and quality of films are pressure of gas, carrier gas flow, concentration of precursors, substrate surface quality and the reaction temperature. When temperature is low, growth is restricted by the surface reaction kinetics whereas at intermediate temperature it is determined by reacting gases being supplied to the substrate. At high temperature, reduced growth rate is observed because of desorption of precursors from the substrate.[24]

Two ways for deposition on substrates are called hot wall and cold wall setup. (Fig. 6) The deposition can occur even on reactor walls in the hot wall setup which does not happen in cold wall design. Gas phase reactions occur in hot wall design, which are limited in cold wall set up. [24]

There are two growth mechanism of CVD process which considers the possibilities of formation of final product. When P and Q type of precursor atoms/molecules are adsorbed and combine to produce the desired material PQ, this is known as Langmuir-Hinshelwood (L-H) mechanism. (Fig. 7). When P adsorbs Q from gas phase and interact with P, Elay–Riedel (E-R) mechanism does not allow sites to be shared (Fig. 6 a,b). As an evidence from the growth rate curve, growth rate is maximum for L-H when P/Q is in balance whereas in E-R, the growth rate keeps on increasing with P/Q.

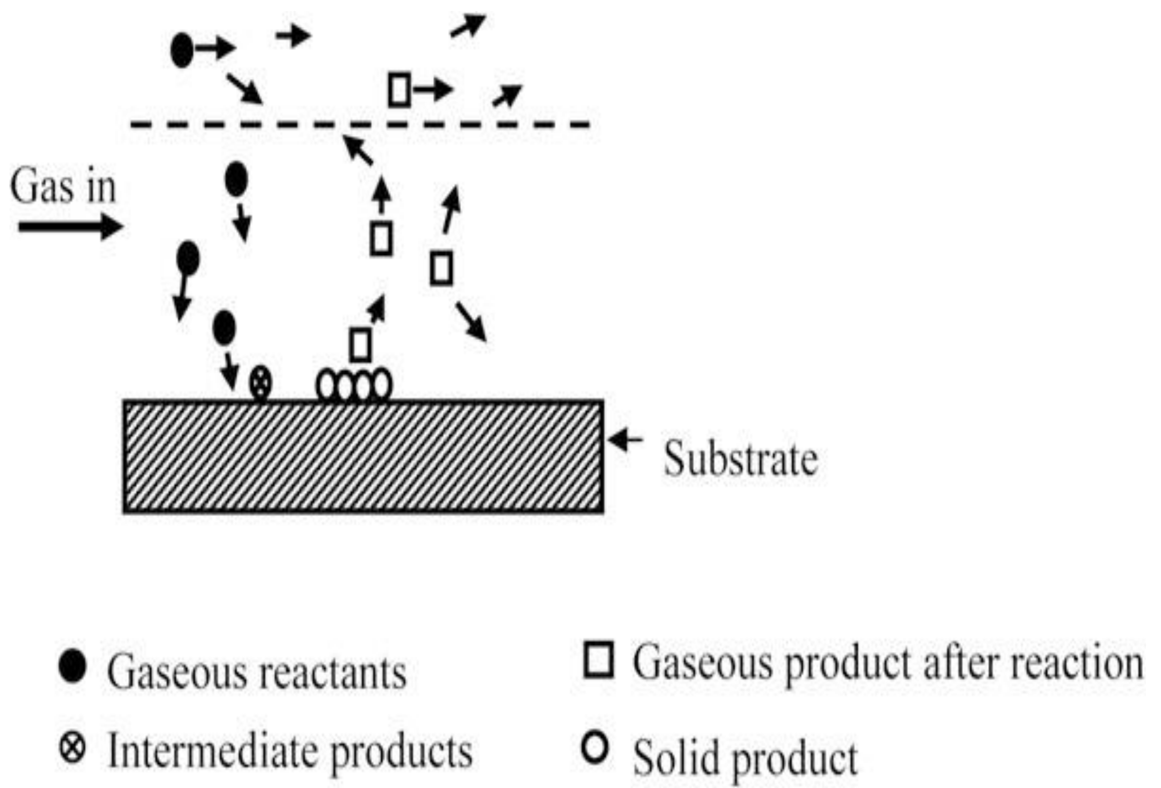


**Fig. 5:** Basic CVD growth process. [24]

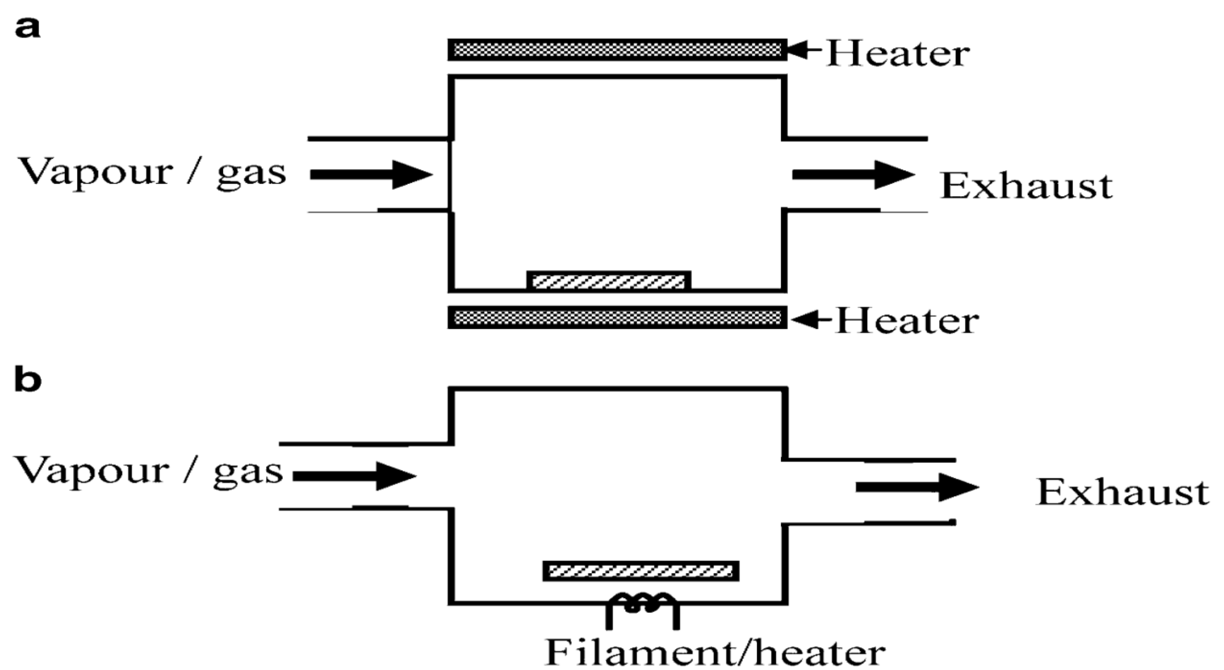


**Fig. 6**: (a) Hot wall CVD setup (b) Cold Wall CVD setup [24].

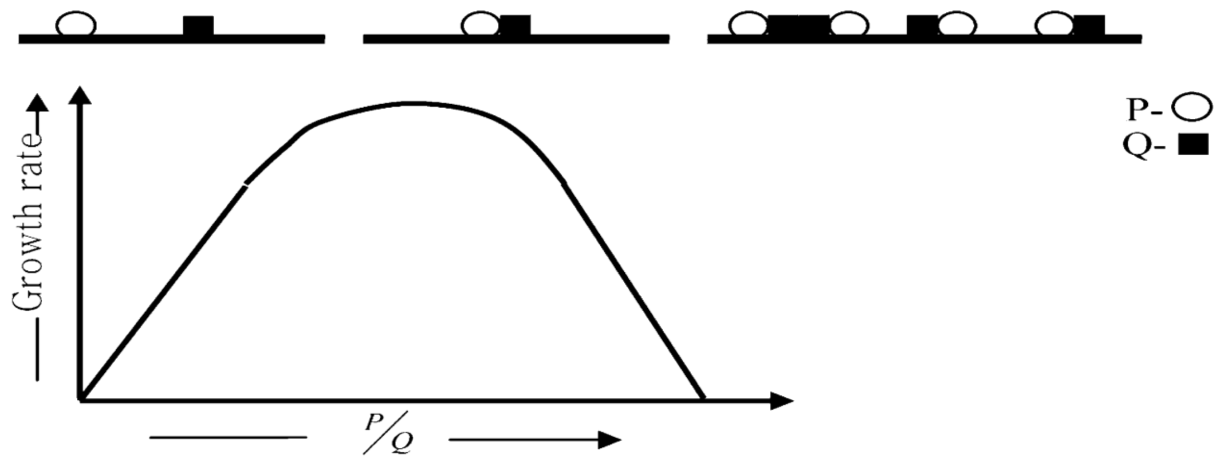


**Fig. 7 a** : Explaining Langmuir-Hinshelwood mechanism [24]

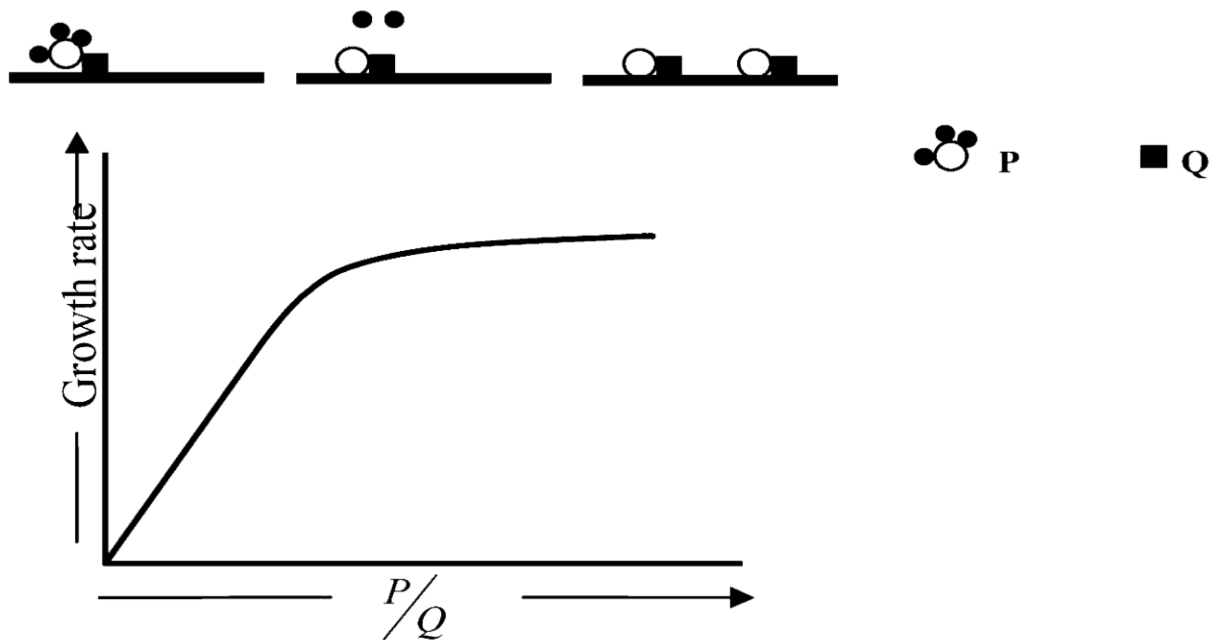


**Fig. 7 b :** Explaining Elay–Riedel mechanism [24].

**1.3: Characterization :**

Investigation of molecular and vibrational structure of TMDCs is inherently challenging due to nanoscale sample. However, recent research has enabled their identification and characterization and manipulation using various tools. Optical microscopy is used to identify the layers fomed initially. Based on the contrast of films fomed on a particular substrate, an estimate of layer thickeness is made [23].

Sapphire and $SiO_2$/Si substrates are used to grow and exfoliate single and few layers of TMDCs. The interference effect from reflection off of the two surfaces of the dielectric on substrate can be identified using the color contrast between substrate and thin films [25]. The maximum limit for the coating to have an optimal contrast is 5 nm. Although this method can be used for known films, for a new material it is necessary to first experimentally verify the monolayer using advanced characterization tools such as Raman, Photoluminiscence (PL) for initial determination, which can be used as a reference for later purposes. This is because index of refraction of new materials are not reported and can lead to ambuguities.

Instead of visual identification of monolayers through optical contrast, fluorescence microscopy can be used. TMDC such as $MoS_2$, $WS_2$ are direct band gap semiconductors when thinned down to single layer, which enable the direct visualization by fluorescence microscopy [26].

Raman spectroscopy is a widely-used characterization tool for fingerprinting 2D materials. When light is scattered from a molecule or crystal is elastic and inelastic scattering happen. In case of elastic scattering, incident photos do not lose energy in the process, which is known as Rayleigh scattering. However, when there is a change in the frequency of scattered photos from incident ones, this process of inelastic scattering is termed Raman scattering. Raman scattering is susceptible to vibrational, rotational or electronic energy of a molecule and is used to determine the layer numbers in TMDCs [28].

When layer number between single, few and bulk substratum is varied, because of difference in interlayer interactions, the raman spectra divaricate from spectral width and intensity [27]. As the vibrational structure of 2D material changes depending upon the number of layers, Raman spectroscopy allows identification of the number of layers. The raman feature for $MoS_2$ are $A_{1g}$ (in plane) and $E_{2g}$ (out of association with plane) vibrational mode. Depending on the relative separation between two peaks, number of layers can be found.

When a semiconductor is excited with photons having energy exceeding the band gap, electrons with specific momentum are formed in conduction band while holes are generated in the valence band. Because of mechanisms like coulomb scattering and the interaction with phonons, the relaxation happens along band gap minima. Successively, the

electrons recombine with holes under emission of photons. Photoluminescence (PL) peak occurs because of exciton (electron hole pair) formation and subsequent recombination in semiconducting TMDCs. As single layer TMDCs have a direct band gap, PL peak is highest for single layer, forming another signature to identify the layer number and thickness [26].

Atomic Force Microscopy (AFM), a type of scanning probe microscope (SPM) which measures properties such as friction, height, surface roughness and is used to determine thickness of thin films with nanometre resolution and a precision of 5% [28, 29]. AFMs measure the van der walls forces between a sharp probe and the sample. In view of convolution, lateral resolution of AFM is low (~30nm), up to 0.1nm is the vertical resolution. It can also be used to check the uniformity and surface roughness of deposited layers [28].

Transmission Electron Microscopy (TEM) is accomplished to provide crystallinity and atomic resolution. It is also used to see crystal defects in the sample. [30] Scanning transmission electron microscopy (STEM), with electron energy loss spectroscopy (EELS) can be designed to picture individual atoms in a thin film. 2D materials being one atom thick provide an interesting surface to be investigated using these advanced tools.

Scanning Tunnelling Microscopy (STM) works on the principle of tunnelling of electrons from substrate to tip and vice versa. STM is widely used to quantify the structure of sample electronically and topographically. STM is also employed to manipulate single atoms at given points of materials and can be used to create nanostructure of desired order [31].

Angle Resolved Photoelectron Spectroscopy (ARPES) is a type of photoelectron spectroscopy which is established on the photoelectric effect originally observed by Hertz. ARPES is capable of directly resolving resolve electronic band structures of materials in the crystal momentum space. Specifically, since ARPES relies on alignment of the probed materials in respect of beam and detection, it can be used to evaluate possible epitaxy of the grown layer with the substrate [32].

X-ray photoelectron spectroscopy (XPS), addressed to a method which is surface-sensitive and quantify the empirical formula, elemental composition, chemical and oxidation state of the elements that forms a given compound. A beam of photons in X-rays

range of wavelength is irradiated on the material and kinetic energy of the escaping electrons are measured simultaneously [33].

| S.N. | Characterization Tool | Measured property |
|---|---|---|
| 1. | Optical Microscopy | Initial identification based on contrast |
| 2. | Raman Spectroscopy | Number of layers |
| 3. | Photoluminescence | Number of layers |
| 4. | AFM | Thickness of layers |
| 5. | TEM | Crystal structure and atomic resolution |
| 6. | STM | Electronic and topographic structure |
| 7. | XRD | Crystal structure and constituents |
| 8. | ARPES | Resolve energy momentum space |
| 9. | XPS | Chemical state, elemental composition, empirical formula |

**Table 1:** Summary of commonly used characterization techniques

**1.4: Field Effect Transistors:**

The electrical behaviour of field-effect transistor (FET) is regulated by applying an electric field externally. As they involve single carrier type, these are also known as unipolar transistors. There are 3 terminals in FETs: Source, Drain and Gate. The terminal through which carriers enter the channel is called source(S) and the current is designated by $I_s$. Current ($I_d$) leave the channel through the terminal named drain (D).

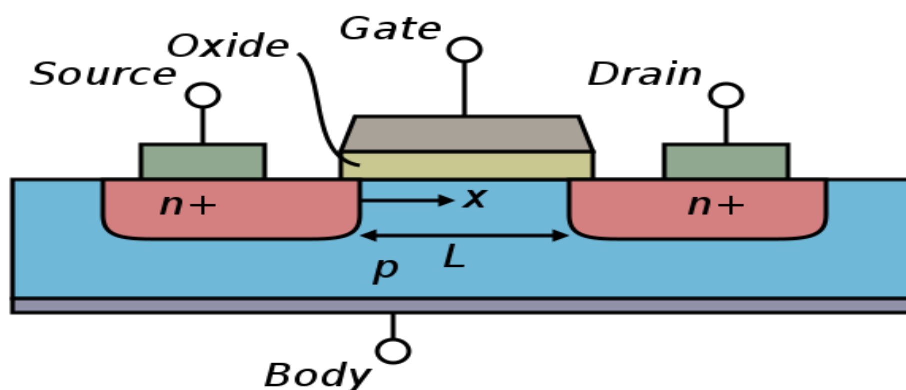


**Fig. 8:** Schematic of an n-type MOSFET

The terminal which modulates the channel conductivity is Gate (G). The conduction of electrons from drain to source terminal is controlled by an electric field in

the device, generated from the voltage difference between body (fourth terminal of FETs, referred as B) and G. The distance between source and drain is size of the gate (L) and extension of the transistor perpendicular to the cross section is called width (W) (Fig. 8).

There are two configurations in FETs which are called top contact and bottom contact. (Fig. 9). When source and drain electrode is on the top of semiconducting material (Fig. 9a), it is called top gated and when they are evaporated on the dielectric before depositing the material, it is called bottom gated. Gate voltage ($V_G$) through the dielectric. induces an electric field resulting in accumulation of charges at semiconductor interface; this can be used to measure current between the source and the drain ($I_{SD}$) by applying a source–drain voltage ($V_{SD}$)

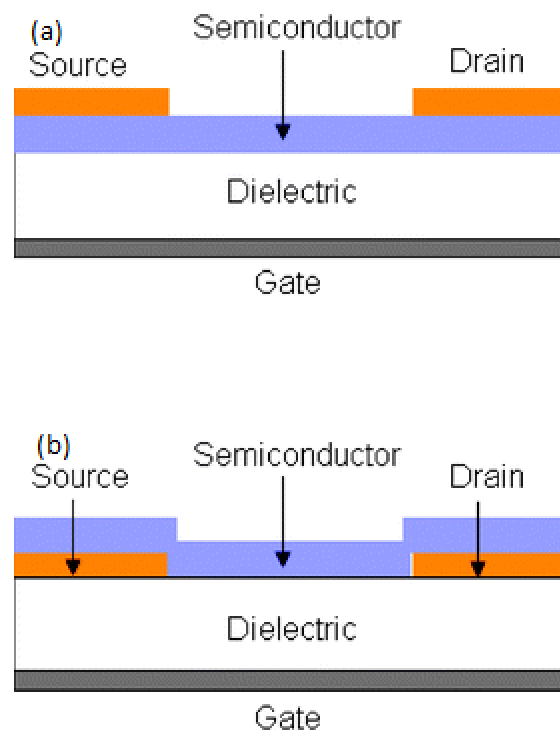


**Fig. 9:** Possible FET configurations: (a) Top contact. (b) Bottom contact. [34]

The nature and quality of the 2D material is an essential requirement to achieve high device performance. Carrier mobility (μ), a measure of the carrier drift velocity upon applying electric field is an important parameter to know the device performance. Another parameter is on /off ratio, a ratio of accumulation mode current about depletion mode current. The gate voltage at which conduction channel starts to form, termed as threshold voltage ($V_T$) is another important parameter to know the electronic properties of material.

# Chapter 2: Experimental Methods

## 2.1: Conventional Growth:

Before proceeding to proposed setup, growth conditions for conventional method to grow $MoS_2$ were optimized to set parameters for the new proposed method. In the conventional CVD approach to grow large area $MoS_2$ atomic layers, substrate is kept facing $MoO_3$ (Fig. 10) which leads to deposition of $MoS_2$ via chemical reactions between the two precursors on the top down face. (Substrate facing precursor) $MoO_3$ (99.98 %, Sigma-Aldrich) and S powders in two separate ceramic boats were used as precursors (Fig. 10).

The precursors $MoO_3$ (99.98 %, Sigma-Aldrich) and Sulphur (99.98 %, Sigma-Aldrich) are kept in 2 separate ceramic boats in a hot wall 2" CVD furnace where nitrogen in used as a carrier gas, whose flow rate is regulated externally using mass flow controller. The sapphire (0001) substrate is kept on the boat face down towards the $MoO_3$ powder (22 mg) and sulphur (220 mg) boat is kept upstream to the flow of carrier gas. The distance between $MoO_3$ and S boat is 15 cm. After keeping the substrate, precursors and boats, the tube is purged at 400 standard cubic centimetres per minute (sccm) of $N_2$ gas flow for 60 minutes. The gas flow is reduced to 200 sccm when the tube is heated to 300 for 5 minutes upto 600˚C. The reaction temperature is 775 ˚C for duration of 10 minutes and the flow of gas is 10 sccm during the temp. range 600-775 C. The tube is opened at 600 sccm after the reaction for a rapid cooling and the termination of reaction.

During the $MoS_2$ growth, $MoO_3$ in the vapour phase undergoes a two-step reaction, where $MoO_3$ gets reduced to $MoO_{3-x}$ ($0 \leq X \leq 1$) during the reaction as an intermediate phase and this can produce $MoS_2$ via various roots. (Fig. 11) $MoO_{3-x}$ can react with sulphur and form $MoS_2$ (Route 2 in fig. 11) or it can from Alpha $MoS_3$ (Route 5 in fig. 11) which can from $MoS_2$ depending on the reaction parameters in presence of $N_2$ gas. So, the deposition of film is a balance between reduction of $MoO_3$ and sulfurization of reduced intermediate phase.

$MoS_2$ layers are formed via the reaction of solid $MoO_3$ and S precursors. The reaction is governed by the equations [23, 35, 36]

$$MoO_3 + x/2\ S \rightarrow MoO_{3-x} + x/2\ SO_2$$

and

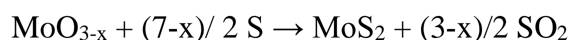

$$MoO_{3-x} + (7-x)/2\ S \rightarrow MoS_2 + (3-x)/2\ SO_2$$

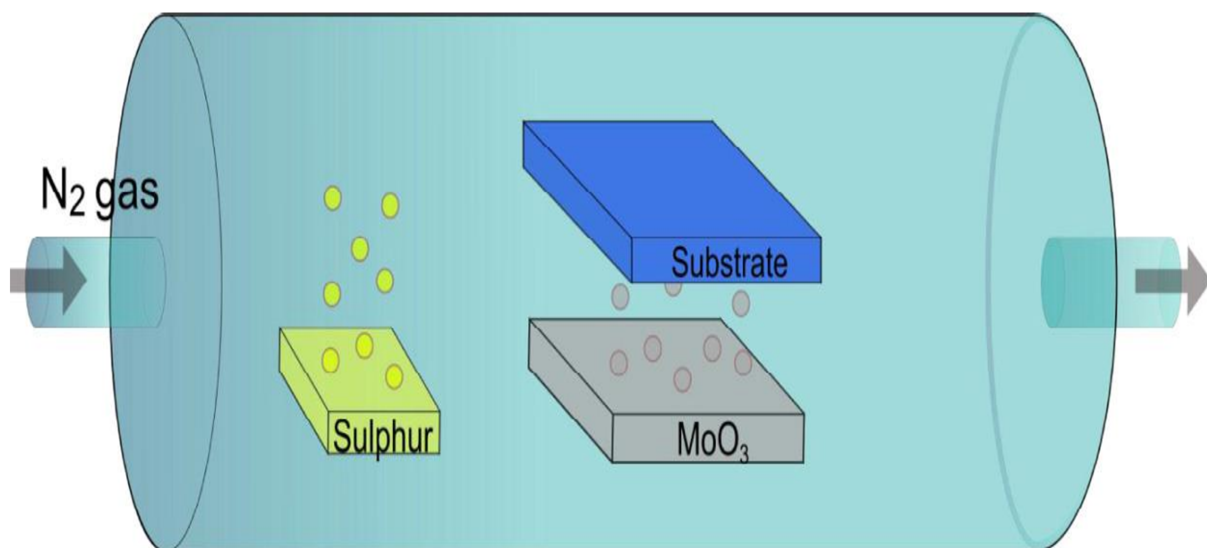


**Fig. 10:** Conventional CVD setup to grow $MoS_2$

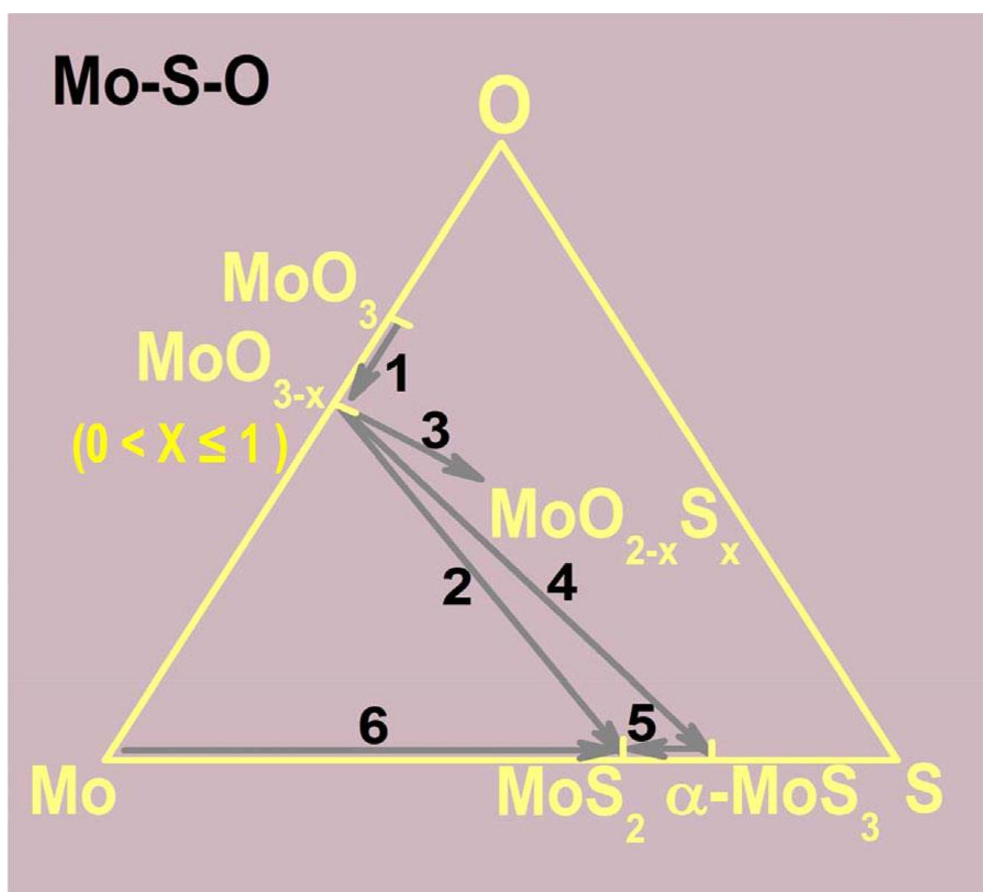


**Fig. 11:** Phase diagram for the possible pathways to produce $MoS_2$. [37]

## 2.2: Proposed new method:

To get large scale and high quality films of $MoS_2$, we propose a new CVD method, altering the geometry of conventional method to yield monolayer single crystal $MoS_2$ films with large and uniform grain size. The novelty of this recipe is the way in which nickel foam of size 3.5 cm × 3 cm with thickness 0.7 µm is used as a barrier membrane to promote homogenous spread of reactants. (Fig. 12) This setup regulates gaseous flow of precursors reaching the substrate surface; thereby decreasing the high nucleation of $MoO_3$ reaching to the surface and results in clean deposition i.e. less unreacted Mo oxide residue, having lesser second layer nucleation as compared to the conventional method.

The mechanism of this particular setup is quite different from the conventional method. In this particular setup, $MoO_3$ after getting reduced to $MoO_{3-x}$ reflects from the closed end of the boat reacts with sulphur and gets deposited on the top face of sapphire substrate. To take care of the flow from open side, the foam is kept sufficiently large in size to cover the edge. Since the flow from closed end comes from the reflection, deposition follows a gradient which follows a decreasing pattern going from the closed end to the open end. This particular geometry leads to uniform flow of $MoO_3$ which results in attaining larger grain size and relatively less thick areas which is not possible in the conventional setup.

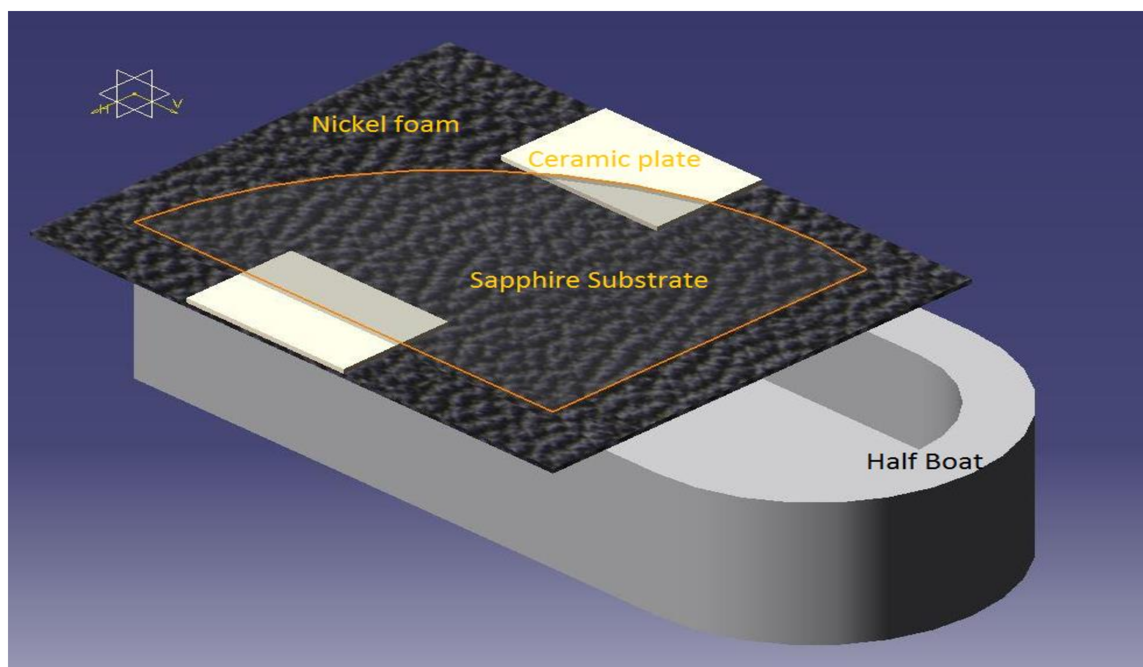


**Fig. 12:** Proposed new setup geometry showing the half boat and substrate placing. $MoO_3$ precursor is beneath nickel foam.

Sapphire substrate was first sonicated in acetone and isopropyl alcohol (IPA) for 3 minutes each and then annealed to 1050 ˚C in air which leads to terrace formation and the amorphousness of the surface decreases compared to the unannealed one and is suitable for the film deposition [38, 39].

Annealed samples are transferred to the CVD system and growth is performed with the setup shown in Fig. 10 with the new setup (Fig. 12) and is based on the gas phase reaction between $MoO_3$ and sulphur evaporated from solid sources using nitrogen as the carrier gas. The ceramic boat containing 15 mg $MoO_3$ (>99.9%, Alfa Aesar) and another boat containing 0.3 g S (>99.9%, Alfa Aesar) was placed in the entrance of a hot wall 2" CVD furnace (Fig. 10) where nitrogen in used as a carrier gas, whose flow rate is regulated externally using mass flow controller. After the purge for an hour in 400 sccm of $N_2$ gas, temperature was set at 300°C with 200 sccm for 10 min. It was then ramped to 800°C at 10 sccm of carrier gas flow, set the temperature to 800°C for 10 min and then cooled down to 600°C with 10 sccm gas flow. The gas flow was increased to 200 sccm and furnace chamber is opened for rapid cooling. (Fig.13).

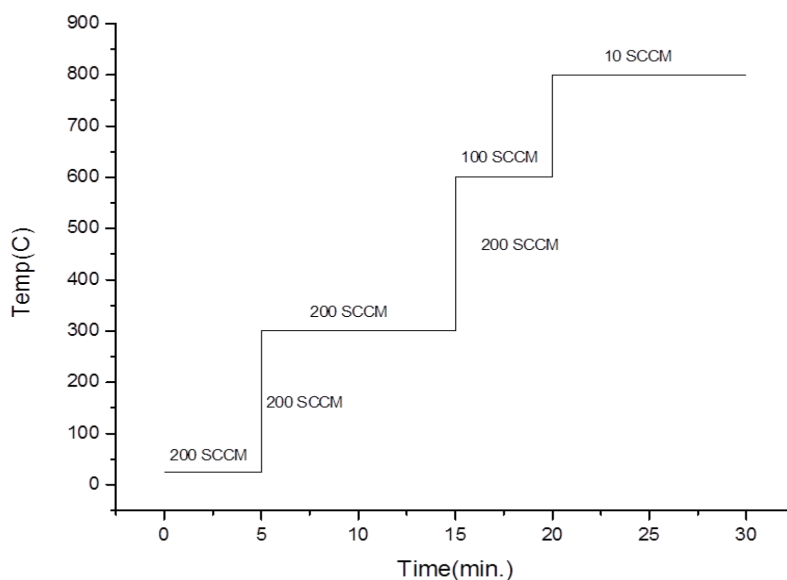


**Fig. 13:** Temperature Vs Time curve for different steps of the reaction. The label shows the $N_2$ flow rate during the various stages of the reaction.

## 2.3: Device fabrication:

To measure the electronic quality of layers formed, top gated Field Effect Transistors (FETs) were fabricated on single-layer $MoS_2$. Top-gated $MoS_2$ FETs were fabricated as follows.

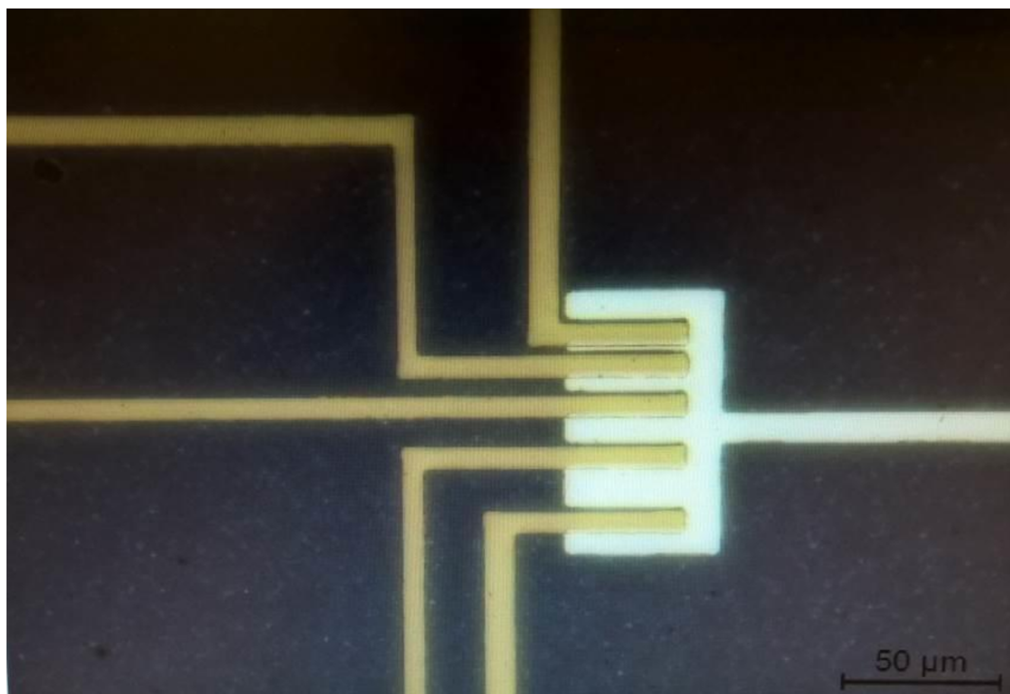


**Fig 14**: Optical image of Top-gate FET fabricated on $MoS_2$ single layers

$MoS_2$ monolayers were identified from their optical contrast, Raman and PL spectroscopy. For fabrication of FET, sample was spin coated with AZ5214E positive photoresist at 5000 rpm for 45s and the resist was cured later at 95· C. After the cure, UV light was exposed to the sample using SUSS mask aligner with premade mask for pattern generation for 1s (Power approx. 1000W). Sample was developed in AZ developer for 40s.

Metal contacts Cr (3nm)/ Ti (10nm)/ Au (20nm) were deposited using e-beam evaporator followed by lift off using acetone bath overnight. To remove the residues, annealing was done in forming gas (Ar (200 sccm) / $H_2$ (20 sccm)) for 2 hrs. $Al_2O_3$ which is used as a gate dielectric was deposited using atomic layer deposition (ALD). Spin coating, exposure to UV light and development of sample was done again for top gate pattern. Cr (2nm) / Au (20nm) were deposited by lift off using acetone bath overnight. Post fabrication anneal was followed after that. The channel length (L) and width (W) of the device are 6 and 40 μm respectively. Top gate dielectric ($Al_2O_3$) thickness is 28 nm. (Fig. 14)

# Chapter 3: Results and Discussion

## 3.1: Optical Characterization:

### 3.1.1: Conventional method:

At the reaction temperature of 775 °C, ambient pressure and carrier gas flow of 10 sccm, optimal conditions for conventional growth are achieved which gives us triangles of previously reported size [23] (Fig. 15). As seen from optical images, reaction temperature of 775 ˚C yields the largest triangles among all the temperature ranges with the precursor concentrations of 10 and 300 mg of $MoO_3$ and sulphur respectively.

The single- crystal flakes were identified by their optical contrast and characteristic triangular shape. For 700 ˚C, triangles of sizes upto 30 µm and continuous area of 2000 µm × 200 µm are observed. At 750 ˚C, triangles of sizes upto 10 µm and continuous area of 1000 µm × 50 µm can be seen using optical microscope. 775 ˚C yields triangles of sizes upto 40 µm and continuous area of 2000 µm × 200 µm with overall coverage of 60 %. At 800 ˚C, triangles of sizes upto 15 µm and continuous area of 500 µm × 100 µm are observed. (Fig.15)

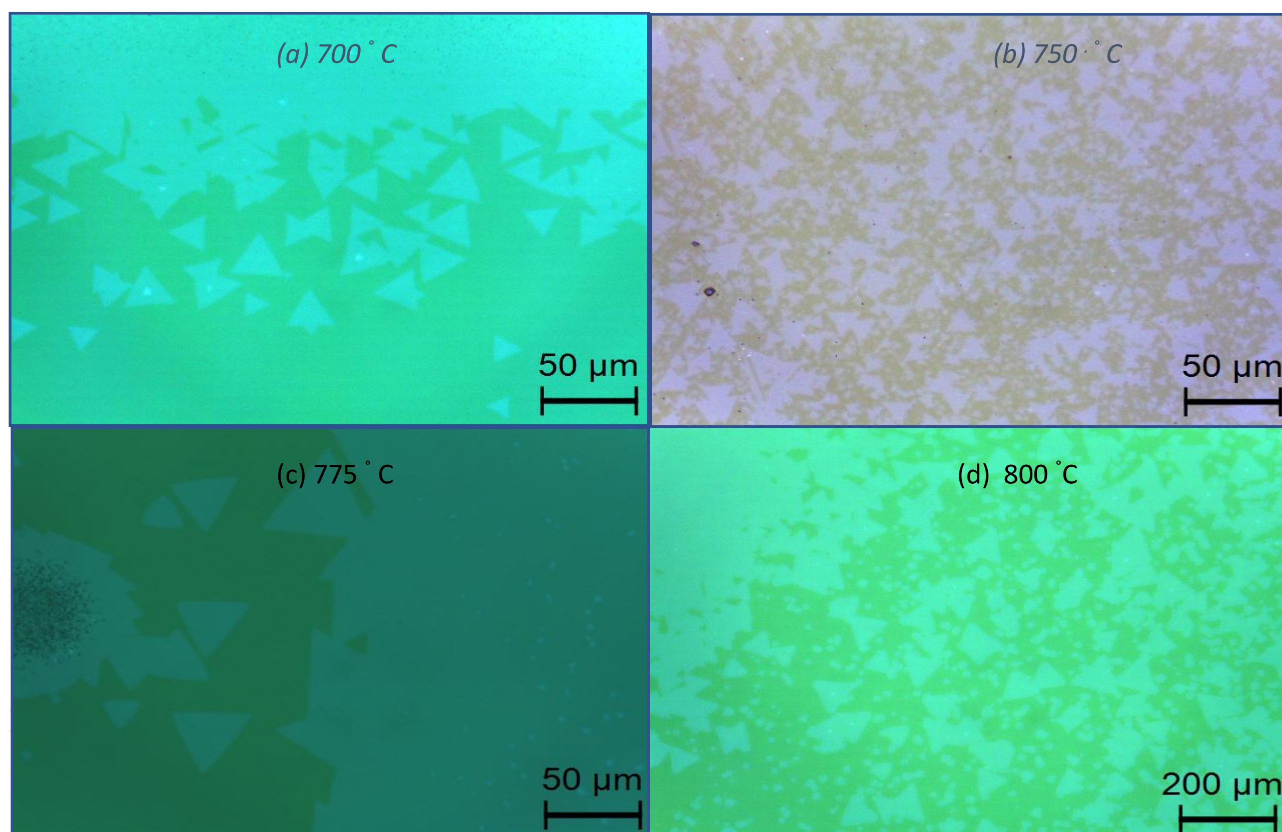


**Fig. 15:** Optical Images of monolayer $MoS_2$ at various temperatures:
(a)700 ˚C (b) 750˚ C (c) 775˚ C (d) 800˚ C

In Fig. 16, 17 the two peaks at 412 $cm^{-1}$ & 393 correspond to $A^{1g}$ & $E^{2g}$ peak respectively. (Excitation wavelength of 532 nm and grating used was 1800 g/mm). The relative peak separation of 19 $cm^{-1}$ confirms the formation of monolayers. PL peaks are associated (Excitation wavelength of 532 nm and grating used was 600 g/mm) with the direct gap transition at K (K′) point [9], and the energy difference between the 1 and 2 peak corresponds to the valence-band splitting due to the strong spin–orbital interaction. Therefore, comparing the data considering triangle size, continuous monolayer formed, overall coverage, raman peak separation, PL peak intensity as the parameters, 775° C proves out to be the optimized temperature for conventional setup. Table 2 summarizes the discussion.

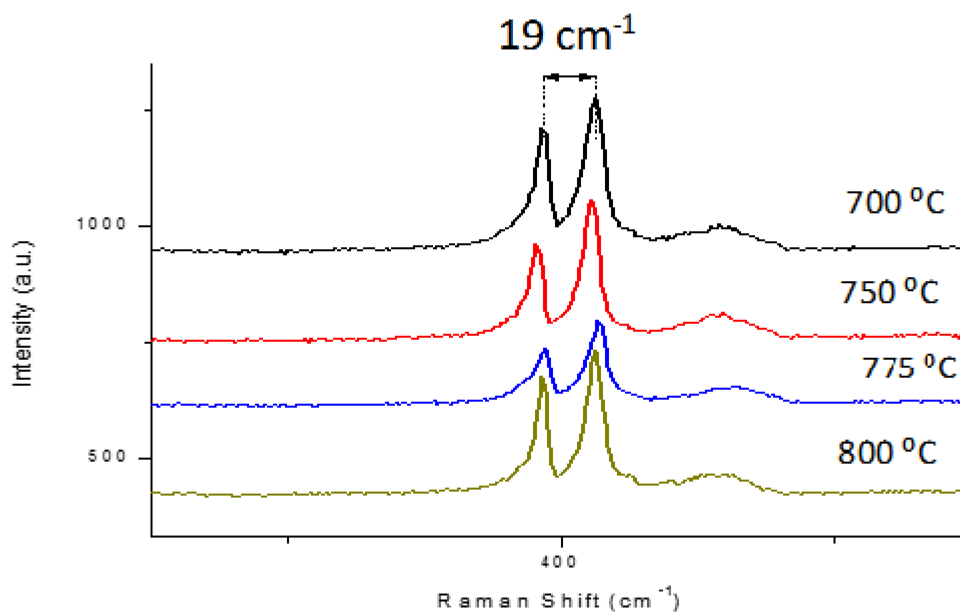


**Fig. 16:** Comparison of Raman Peaks of $MoS_2$ at different temperatures.

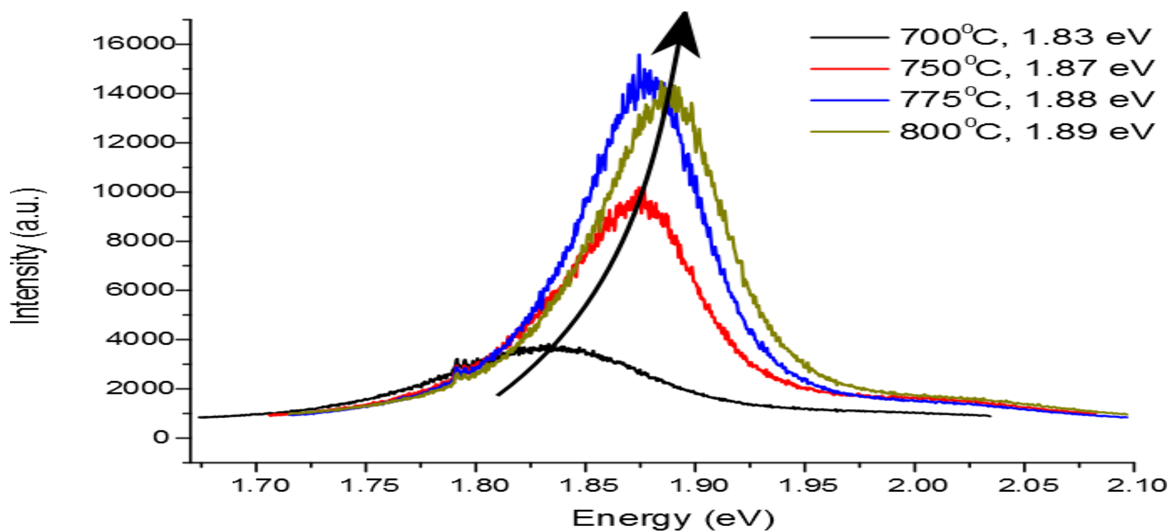


**Fig. 17:** Comparison of PL Peaks of $MoS_2$ at different temperatures.

| Temp.(C) | Isolated Triangle Size(μm) | Continuous Layers(area $\mu m^2$) | Overall coverage (%) | Thicker layers | Raman Peak separation($cm^{-1}$) | PL peak intensity(a.u) |
|---|---|---|---|---|---|---|
| 700 | 10-20 | 2000×200 | 40 | Least | 18.6 | 3000 |
| 750 | <10 | <100×50 | <20 | Less | 18.8 | 8000 |
| 775 | 10-40 | 2000×200 | 50-60 | Not much | 19.1 | 15000 |
| 800 | <15 | 500×100 | 30-40 | Huge | 20 | 13000 |

**Table 2:** Summary of reaction temperature optimization for conventional setup.

The major drawback of this method is its inability to produce large scale films and less coverage which is quite essential from an industry and application point of view. In conventional approach, since the substrate is facing the precursor directly, we see a huge nucleation at the centre, reducing the effective available area of a regulated and uniform growth. (Fig. 18) Other issue which originates from the direct exposure of precursor to the substrate is the excessive nucleation which leads to random growth and there is no specificity and control to the spatial growth. This also leads to thicker layers and not so high quality films. To tackle these issues, we have proposed a new method, an alteration to the geometry of the precursors and substrate which allows us to get large scale as well as layers clean of thicker layers and unreacted Mo oxide.

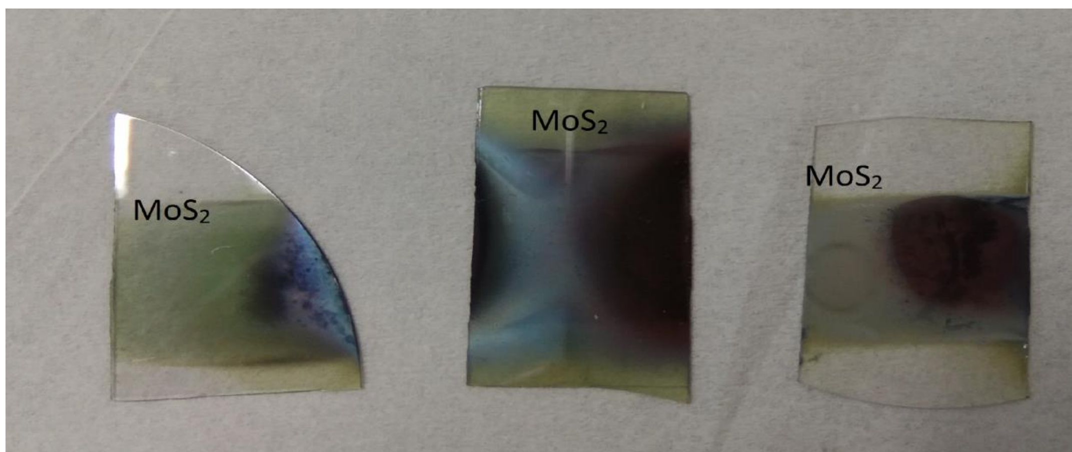


**Fig. 18:** Camera image of $MoS_2$ grown on sapphire using conventional setup where yellow colour is $MoS_2$. (At 775 ˚C)

### 3.1.2: Proposed new method:

A higher temperature of 800 ˚C was used in this method to counter the barrier and make the precursor escape it easily. Optical microscopy image of grown films of $MoS_2$ by the proposed growth model as shown in fig. 19 shows that $MoS_2$ thin films deposited on sapphire substrates are light yellow-green exhibiting obvious colour contrast with transparent bare sapphire substrates.

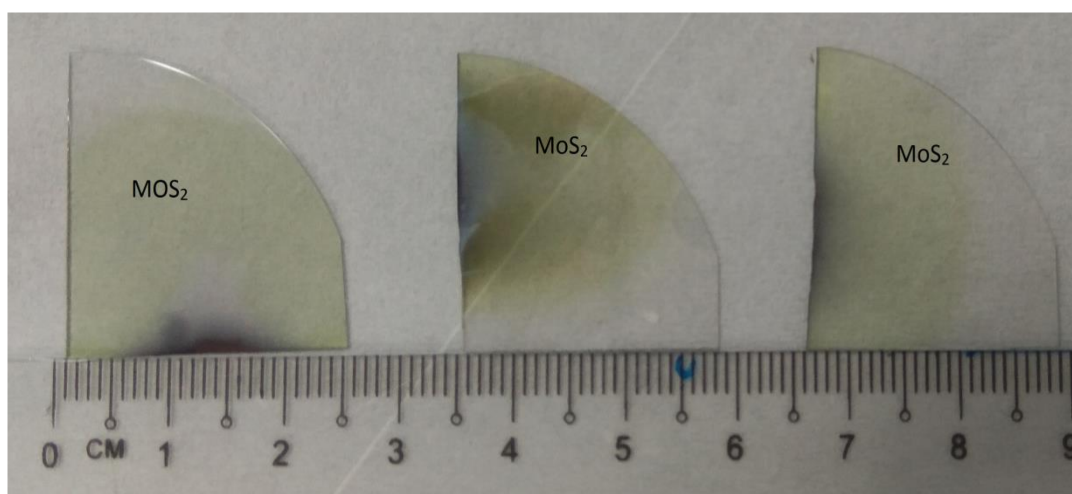


**Fig. 19:** Camera image of $MoS_2$ grown on cm scale sapphire using proposed method where yellow colour is $MoS_2$. (At 800 ˚C)

As per the mechanism explained in the last chapter, the growth happens on the other side of the substrate i.e. surface facing away from precursors. Optical image shows that (Fig.20) this new method not only leads to relatively less thick areas but also provides a large effective area for growth. The open end of the half boat helps the sulphur to reach $MoO_3$ and reduce it during the initial part of the reaction. During the latter part of the reaction, when the temperature reaches 800˚ C, this reacts with sulphur to form $MoS_2$ which gets relatively even distribution as compared to the conventional method.

The single- crystal flakes were identified by their optical contrast and characteristic triangular shape. The size of isolated triangles deposited are of size upto 170 μm whereas continues area extends upto mm scale. The films deposited are relatively cleaner i.e. less number of unreacted particles as well as thicker layers compared to conventional method (Fig. 20).

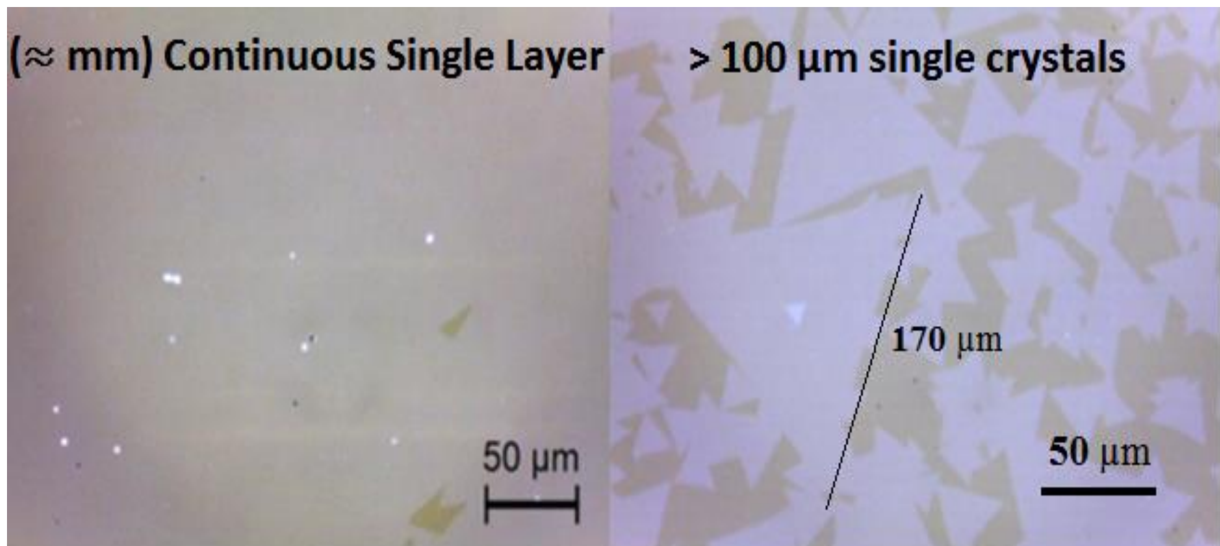


**Fig. 20:** Optical microscope images of mm scale continuous layers and single layer triangles.

To confirm the formation of single layer of $MoS_2$ thin films, Raman spectra of deposited $MoS_2$ thin films was measured. Figure 21 shows the two characteristic Raman $A_{1g}$ and $E^1{}_{2g}$ modes of $MoS_2$ sample. The frequency difference (Δ) between $A_{1g}$ and $E^1{}_{2g}$ modes being 18 $cm^{-1}$ suggests the formation of single layer. [40] As explained in the introduction, in single-layer, being a direct band gap semiconductor $MoS_2$ allows strong PL emission. PL spectra of $MoS_2$ has a peak at around 666 nm (1.9 eV) which suggests the transition from indirect to direct band gap semiconductor and the signature of single layer and provides the confirmation of (Fig. 22) monolayer film growth.

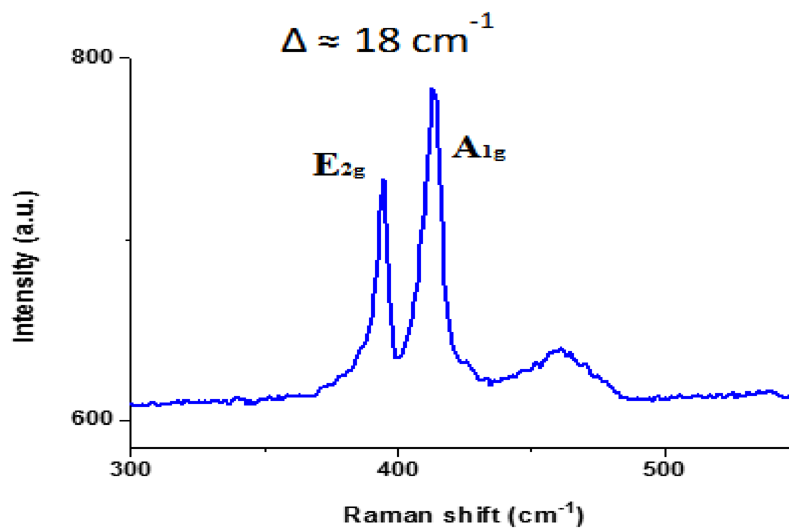


**Fig. 21:** Raman peak separation of two modes confirming the deposition of single layers.

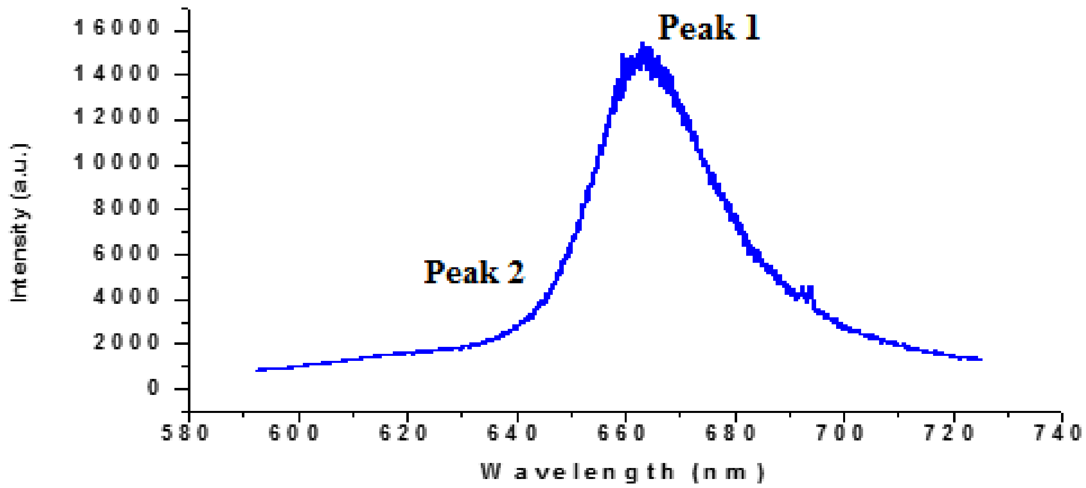


**Fig. 22:** PL peaks at 666 nm (1.9 eV) confirms the formation of single layers.

### 3.2: Raman and PL mapping:

Raman and PL intensity mapping were done to check the homogeneity of the layers deposited on sapphire. The intensity mapping shows takes raman and pl peak at every point of the area measured and the contrast change in the 3d plot is a signature of inhomogeneity of the film deposited.

Figure 23 a, b shows raman mapping of two vibration modes ($E^1_{2g}$, $A_{1g}$) of $MoS_2$ triangular single crystal, acquired with integration times of 0.6 S on taken on 100 *100 points. As seen from 23a, most of the $E_{2g}$ peaks lie in the range of 385-390 nm which is same as previous reports. Similarly, most of the $A_{1g}$ peak lies in the range of most of 410-415 nm which again overlaps with previous reports. Raman mapping of the difference in $E^1_{2g}$ and $A_{1g}$ peaks shows a uniform difference of 19-20 except at the edges, suggesting the single layer being homogenous in the area taken (Fig. 23c) However, significant variations are seen in some areas which correspond to the bilayer, which can be from the colour contrast. The PL intensity mapping (Fig. 23d) supports the implication of Raman data and it can be seen that the edges and some regions within the triangles have higher intensity. Fig.23 e,f shows a characteristic raman and PL spectra of $MoS_2$ single layer

The mapping gives another signature of quality of layers formed spatially. More the homogeneity, it can be applied easily. This proposed method helps to achieve the homogeneity easily.

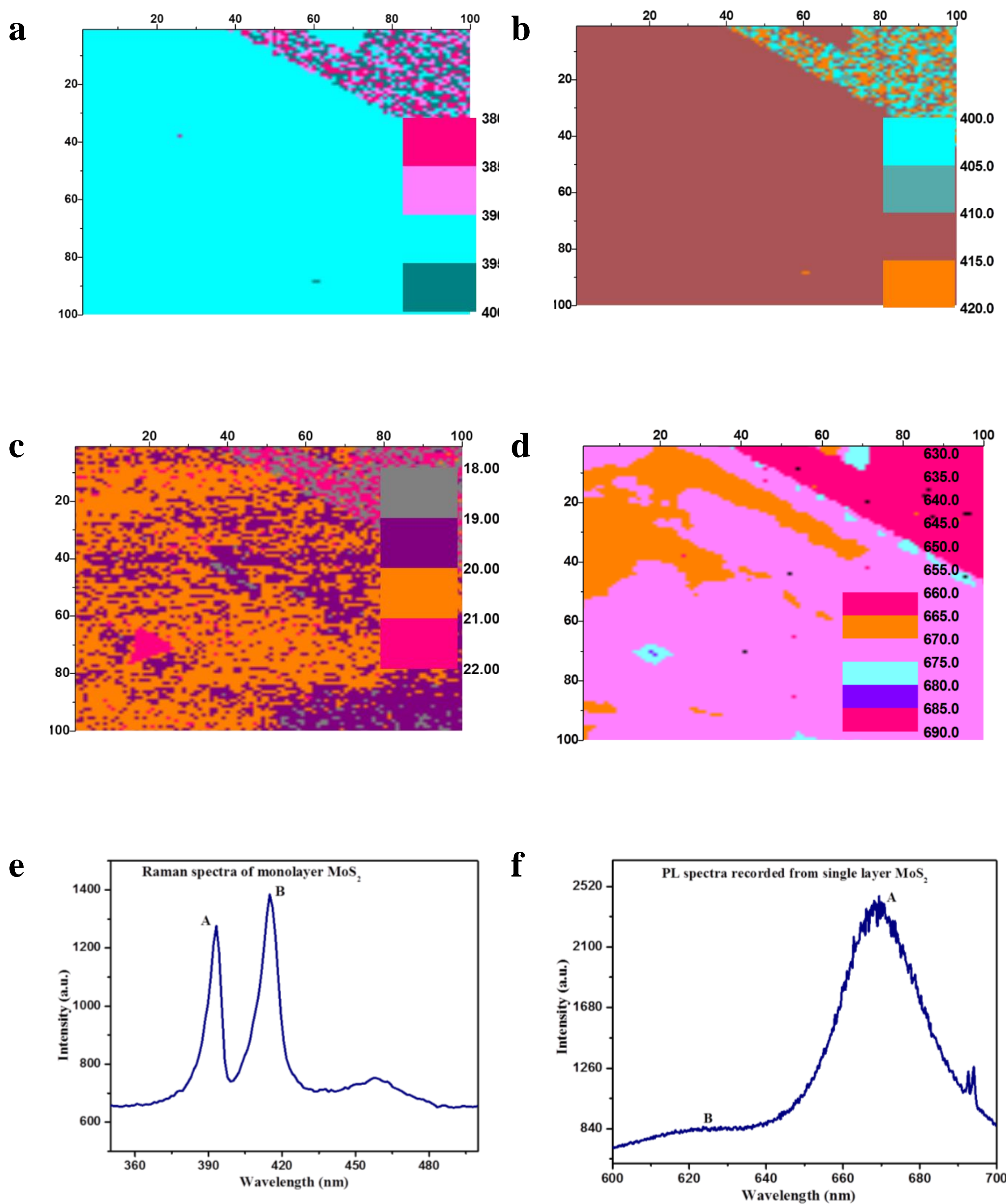


**Fig. 23:** (a,b) Raman intensity mapping at the $E^1_{2g}$, $A_{1g}$ vibrating modes. (c) Raman intensity mapping from the difference between two peaks. (d) PL peak from the A exciton, respectively. Scale bar-3 μm (e) Characeristic raman spectra confirming single layer formation (f) Characteristic PL spectra showing the two exciton peaks.

### 3.3: Atomic Force Microscopy (AFM)

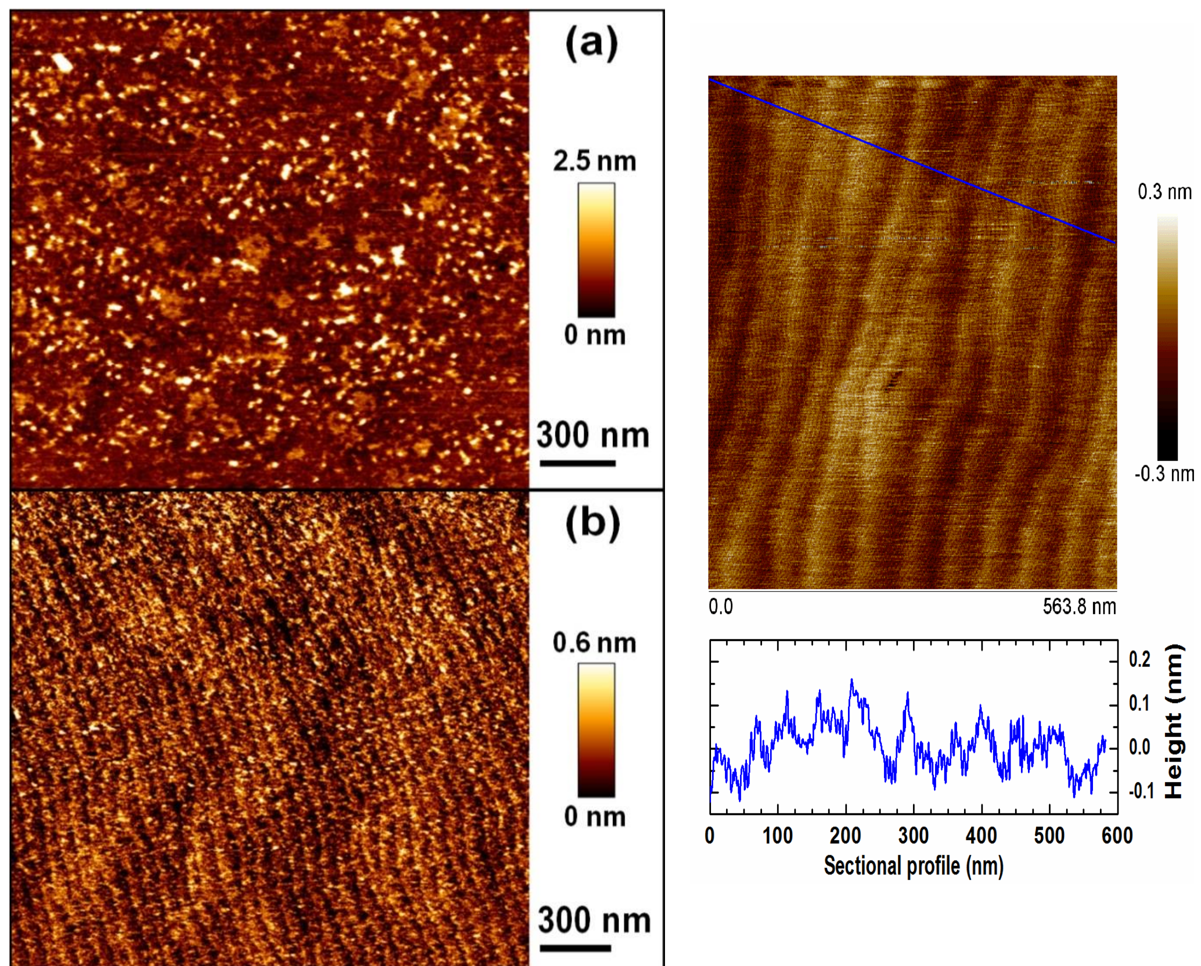


**Fig. 24:** AFM images of sapphire wafers (a) before and (b) after heat treatment at 1050˚ C in air for 60 min [42].

As can be seen from fig. 24, annealing reduces the step height from 0.3 to 0.1 nm. Surface atomic terraces/steps (c/6) are clearly seen after the heat treatment. To measure the thickness of single layer formed, AFM was used. Fig. 25,26 shows image and the height profile taken at the boundary of a $MoS_2$ monolayer triangle. The thickness of the $MoS_2$ layer is measured to be about 0.74 nm, which confirms the monolayer characteristic of layer deposited. As seen from Fig. 24, the $MoS_2$ single layer triangle has a height of 0.74 nm which is consistent with the previous reports. AFM data shows the roughness of single layer to be around 0.1 nm which stems from surface roughness.

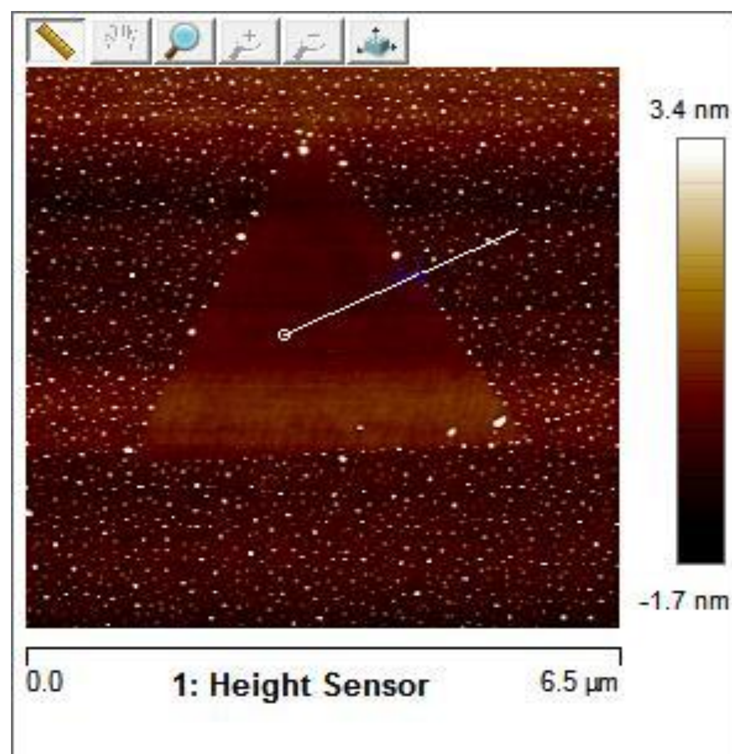


**Fig. 25:** AFM image of $MoS_2$ triangle formed.

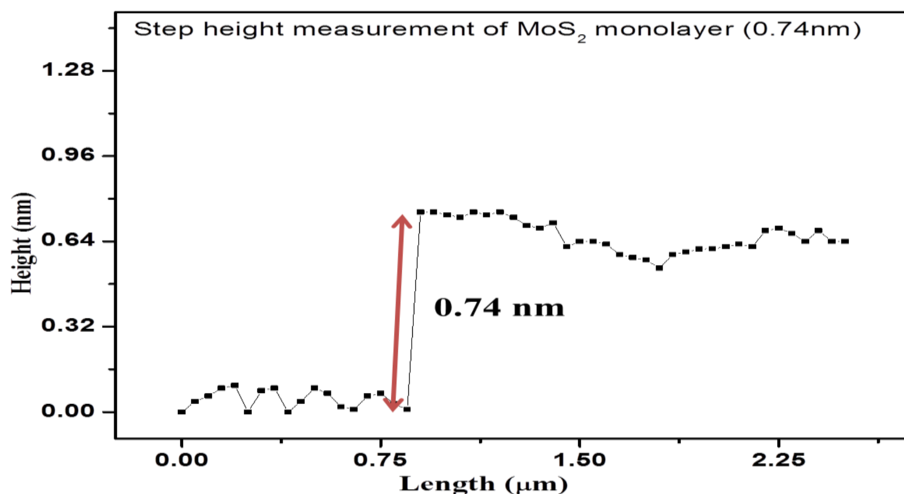


**Fig. 26:** Height profile of single layer shows the thickness to be 0.74 nm.

**3.4: X-ray photoelectron spectroscopy:**

To find the elemental compositions which are related to binding energy of a given element, $MoS_2$ thin films were checked using XPS. As shown in Figure 27, the $MoS_2$ films synthesized using proposed method yields $Mo^{6+}$ binding energies of 230.4 and 234 eV, which correspond to Mo $3d_{5/2}$ and Mo $3d_{3/2}$ respectively, and S binding energies of 163.3 and 164.5 eV, corresponding to S $2p_{3/2}$ and S $2p_{1/2}$, respectively with a 1:2.06 atomic ratio of Mo to S.

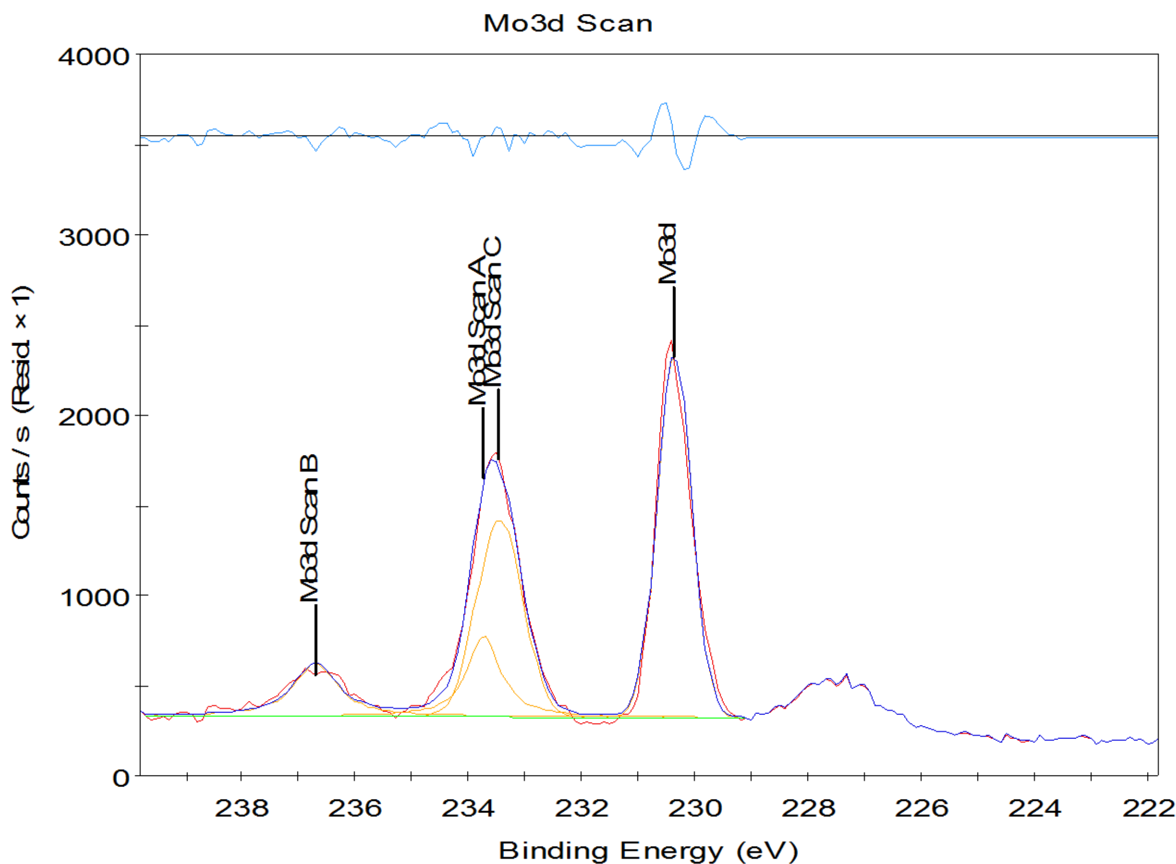


**Fig. 27:** XPS Spectra of Mo 3d peak.

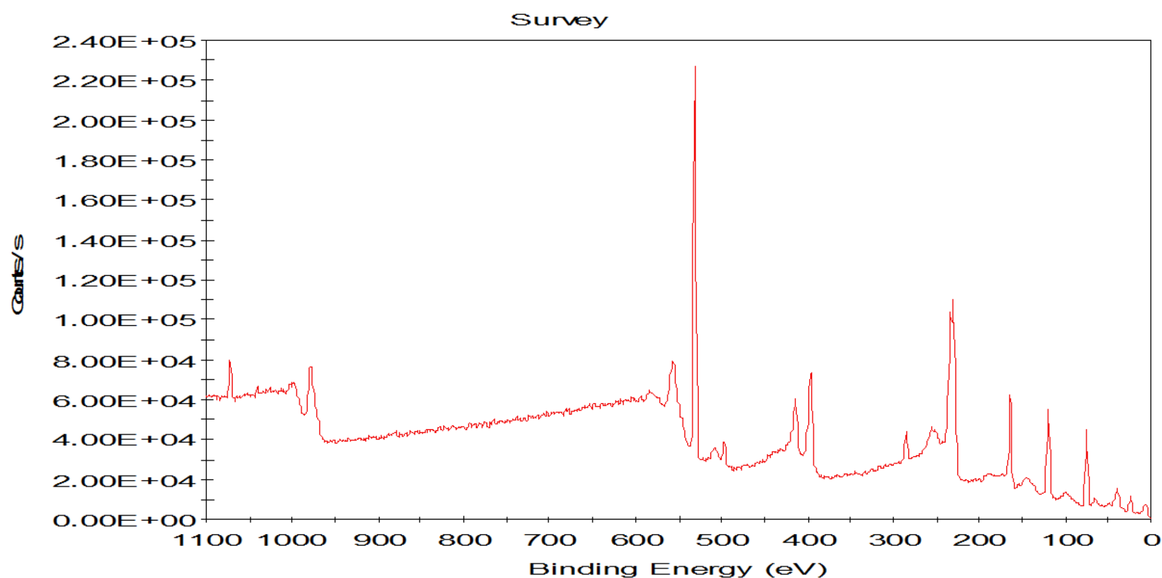


**Fig.28:** Survey on $MoS_2$ thin films showing absence of Ni peak.

The two sets of peak represent the two-oxidation state of Mo (4 and 6), where $Mo^{4+}$ represents $MoO_2$ and $Mo^{6+}$ represents $MoO_3$ (Fig. 28). The absence of nickel (Ni) peak in survey (Fig. 28) the XPS spectra(Ni peak is at approx.. 800 eV) shows that Ni does not

take part in the growth, thereby reducing the possibility of impurities from the filter used. Other elements like Al (from sapphire), C (growth impurity), O (from Mo precursor) were also seen from the XPS. The stoichiometry being close to 2 using this method indicates that at this temperature, less oxide and impurities were formed and the films were produced with a higher crystalline quality than conventional setup, which in turn suggests that this method produces the synthesized film with a better quality.

**3.5: Electrical transport measurements:**

Measurements are performed at room temperature with the source grounded. Top gate width is 40 µm and top gate length is 6 µm.

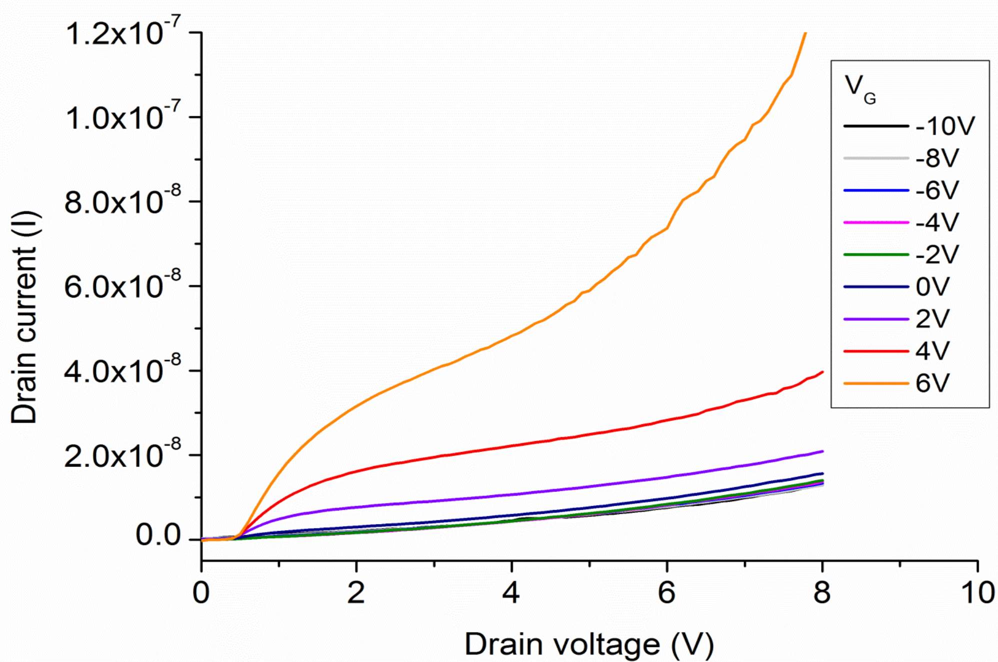


**Fig. 29**: Drain Current ($I_D$) Vs. source drain voltage ($V_{DS}$) of device before anneal showing n type characteristic of $MoS_2$.

From preliminary results, source–drain current ($I_{DS}$) versus top gate voltage ($V_{TG}$) curve recorded from the top-gated device in a for a bias voltage ranging from -10 V to 6 V shows drain currents in the order of $10^{-6}$(Fig.29) Device performance was improved after and anneal at 10%/90% flowing $H_2$/Ar for 2 hours at 200°C. Drain current was improved by an order of 10 for the same drain voltage. (Fig. 30) The device can be completely turned off by changing the top gate bias from −10 to 6 V. For $V_{ds}$ = 0.5 V, the $I_{on}/I_{off}$ ratio is > 404. The mobility of the fabricated device is 0.13 $cm^2$/Vs. (Fig. 31). On off ratio and mobility values are calculated using equations 2 and 3. We have not fabricated enough number of working devices with different channel lengths to calculate contact resistance.

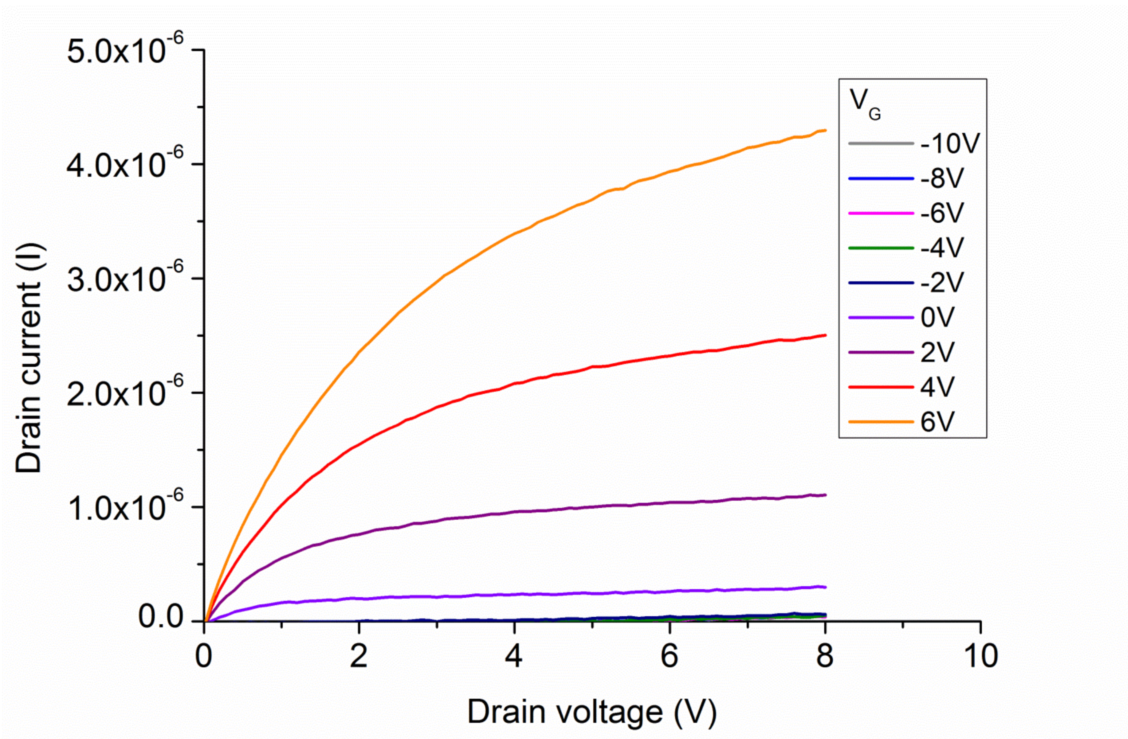


**Fig. 30**: Drain Current ($I_d$) vs. source drain voltage ($V_{DS}$) showing improved performances of device after anneal.

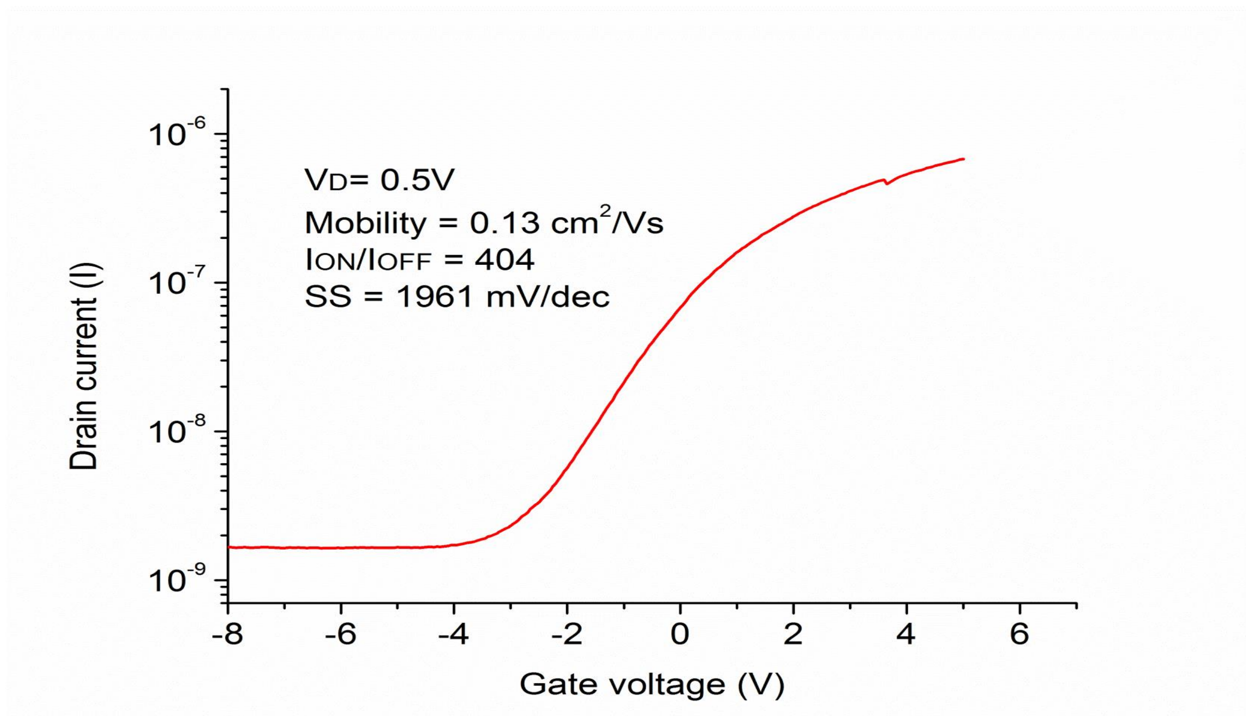


**Fig. 31**: Drain Current ($I_D$) Vs. Gate voltage ($V_G$) showing device after anneal.

State of the art research on 2D transistors has shown the top gate FET electron mobility value to be ranging from 1 to 300 $cm^2\ V^{-1}S^{-1}$ [16]. Occasionally, electron mobility

up to 1000 $cm^2$ $V^{-1}S^{-1}$ has also been reported [41]. The values obtained from the preliminary results is a little low compared to the reports, which is going to further improve with more number of device fabricated, reducing the electrode sample resistance and further optimization.

### 3.6: Advantages of proposed method:

The films deposited by the proposed CVD method not only give large area uniform, impurity and thicker nucleation free triangles, but it also gives a well-defined and reproducible spatial distribution of monolayer compared to conventional methods. Using this property, growth on smaller substrates can be done easily. For example, to study TEM of $MoS_2$, after the growth on substrate, it is transferred to the TEM grid, which by virtue of the wet method leads to impurities. In wet method, $MoS_2$ grown on sapphire is transferred by spin coating PMMA and then using water and etching agent. The method developed gives us a route to grow material directly on TEM grid.

Optical microscopy image shows the triangles formed on a TEM grid which has 8 nm coating of $Si/SiO_2$. Raman and PL spectroscopy confirms the formation of single layer formed. (Fig. 32) TEM image shows the sulphur vacancies in $MoS_2$ formed and can be used as a template to study using advanced characterization tools. TEM imaging is done on Annular Dark Field (ADF) imaging mode which is also called G contrast. This mode shows a contrast proportional to the atomic number of the elements involved. As seen from TEM image, brighter atoms represent Mo and darker atoms are sulphur. No atoms in the TEM image represent the defects in the crystal structure of $MoS_2$ formed (Fig. 33).

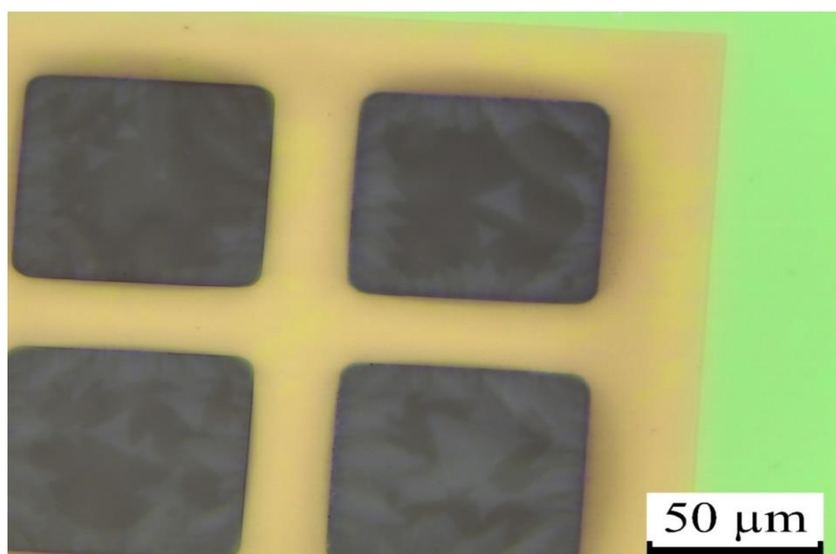


**Fig. 32**: Optical images of $MoS_2$ monolayer triangles grown on a TEM grid using proposed method.

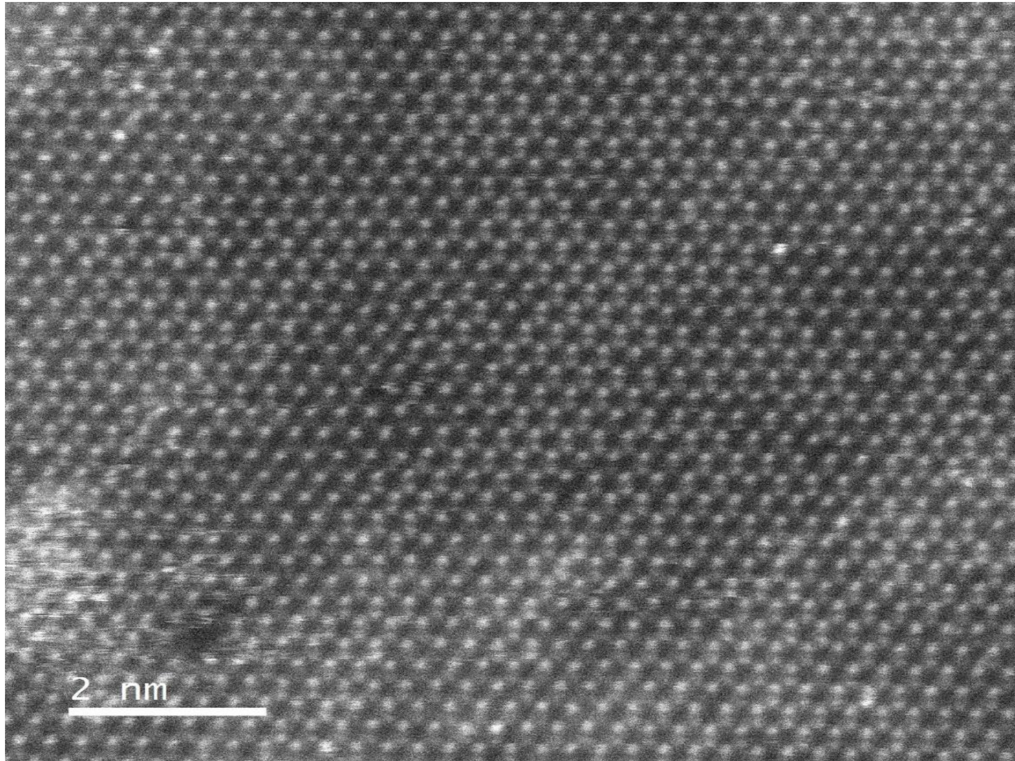


**Fig. 33:** TEM image of $MoS_2$ crystals where bright represent Mo atoms and dark represent S atoms.

The Growth on TEM grid does not only provide a signature of spatial preference of growth of the proposed method, this also provides a route to grow these materials on other small substrates for ex. AlN, HOPG directly.

# Chapter 4: Conclusion and Outlook

## 4.1 Thesis Summary:

In this thesis, an extensive study of CVD growth mechanism of $MoS_2$ has been done. A new method has been proposed which yields single layer triangles which are large in lateral size and larger continuous layers than the conventional approach. Optical microscope was used to identify the single layers formed based on the contrast difference. Raman and PL spectroscopy were applied to verify the formation of single layer and the quality of films formed. Raman and PL mapping were also done to see the homogeneity of the layers formed. AFM was done to check the thickness of the monolayer triangles of $MoS_2$. XPS was used to see the elemental composition and check the impurity in the films grown.

The proposed method gives monolayer triangles upto 170 μm and continuous layers in cm scale. Raman and PL spectroscopy shows the relative difference between two peaks to be around 19 which is consistent with reports. The films deposited are quite homogenous, which comes from the point to point consistent peaks using Raman and PL. AFM shows the thickness of triangles is 0.74 nm which is again consistent with previous reports. XPS shows the elemental composition of triangles formed.

Transport measurements were done by fabricating a 3 terminal FET on $MoS_2$ monolayer and device characteristic were calculated.

## 4.2 Future Work:

Although this thesis has discussed a new method of growth of $MoS_2$ thin films which presents a potential avenue for scaling up to wafer size production for industrial use, there are areas which can be improved. Although this method gives better results than previous reported conventional methods, detailed mechanism of CVD growth of 2D materials has still not been fully understood, which can be instrumental in layer controlled growth of these films. Potential improvements in the setup will be to use a larger boat with a larger substrate and tube, which can result in wafer scale (4cm or more) growth. Foam with different substance having high melting point and different porosity would be useful for this particular setup. Growth wise, this growth setup can be extended to grow relatively new and less studied materials. This method can be generalized to two zone chamber CVD to have more control over the specific spatial heating rate. Detailed characterization using TEM and EELS can be done to see whether this route leads to lesser crystal impurities.

**References:**


1. Novoselov, K.S., et al., *Electric Field Effect in Atomically Thin Carbon Films.* Science, 2004. **306**(5696): p. 666-669.
2. Frindt, R.F., *Single Crystals of MoS2 Several Molecular Layers Thick.* Journal of Applied Physics, 1966. **37**(4): p. 1928-1929.
3. Mas-Balleste, R., et al., *2D materials: to graphene and beyond.* Nanoscale, 2011. **3**(1): p. 20-30.
4. Wang, Q.H., et al., *Electronics and optoelectronics of two-dimensional transition metal dichalcogenides.* Nat Nano, 2012. **7**(11): p. 699-712.
5. Kamihara, Y., et al., *Iron-Based Layered Superconductor: LaOFeP.* Journal of the American Chemical Society, 2006. **128**(31): p. 10012-10013.
6. Geim, A.K. and I.V. Grigorieva, *Van der Waals heterostructures.* Nature, 2013. **499**(7459): p. 419-425.
7. Ayari, A., et al., *Realization and electrical characterization of ultrathin crystals of layered transition-metal dichalcogenides.* Journal of Applied Physics, 2007. **101**(1): p. 014507.
8. Yin, Z., et al., *Single-layer MoS2 phototransistors.* ACS Nano, 2012. **6**(1): p. 74-80.
9. Mak, K.F., et al., *Atomically Thin: A New Direct-Gap Semiconductor.* Physical Review Letters, 2010. **105**(13): p. 136805.
10. Mak, K.F., et al., *Control of valley polarization in monolayer MoS2 by optical helicity.* Nat Nano, 2012. **7**(8): p. 494-498.
11. Zeng, H., et al., *Valley polarization in MoS2 monolayers by optical pumping.* Nat Nano, 2012. **7**(8): p. 490-493.
12. Zhang, Y., et al., *Direct observation of the transition from indirect to direct bandgap in atomically thin epitaxial MoSe2.* Nat Nano, 2014. **9**(2): p. 111-115.
13. Gao, P., et al., *Electrically Driven Redox Process in Cerium Oxides.* Journal of the American Chemical Society, 2010. **132**(12): p. 4197-4201.
14. Nayak, A.P., et al., *Pressure-Dependent Optical and Vibrational Properties of Monolayer Molybdenum Disulfide.* Nano Letters, 2015. **15**(1): p. 346-353.
15. Chhowalla, M., et al., *The chemistry of two-dimensional layered transition metal dichalcogenide nanosheets.* Nat Chem, 2013. **5**(4): p. 263-75.
16. Radisavljevic, B., et al., *Single-layer MoS2 transistors.* Nat Nanotechnol, 2011. **6**(3): p. 147-50.
17. Xu, M., et al., *Graphene-Like Two-Dimensional Materials.* Chemical Reviews, 2013. **113**(5): p. 3766-3798.
18. Ouyang, B., et al., *Phase engineering of monolayer transition-metal dichalcogenide through coupled electron doping and lattice deformation.* Applied Physics Letters, 2015. **107**(19): p. 191903.
19. Yan, R.H., A. Ourmazd, and K.F. Lee, *Scaling the Si MOSFET: from bulk to SOI to bulk.* IEEE Transactions on Electron Devices, 1992. **39**(7): p. 1704-1710.
20. Splendiani, A., et al., *Emerging Photoluminescence in Monolayer MoS2.* Nano Letters, 2010. **10**(4): p. 1271-1275.
21. Taur, Y. and T.H. Ning, *Fundamentals of modern VLSI devices*. 2013: Cambridge university press.
22. Li, X., et al., *Large-area synthesis of high-quality and uniform graphene films on copper foils.* Science, 2009. **324**(5932): p. 1312-4.
23. Najmaei, S., et al., *Vapour phase growth and grain boundary structure of molybdenum disulphide atomic layers.* Nat Mater, 2013. **12**(8): p. 754-759.

24. Kulkarni, S.K., *Nanotechnology: Principles and Practices*. 2007: Capital Publishing Company.
25. Benameur, M.M., et al., *Visibility of dichalcogenide nanolayers.* Nanotechnology, 2011. **22**(12): p. 125706.
26. Splendiani, A., et al., *Emerging photoluminescence in monolayer MoS2.* Nano Lett, 2010. **10**(4): p. 1271-5.
27. Late, D.J., et al., *Rapid Characterization of Ultrathin Layers of Chalcogenides on SiO2/Si Substrates.* Advanced Functional Materials, 2012. **22**(9): p. 1894-1905.
28. Osada, M. and T. Sasaki, *Nanosheet architectonics: a hierarchically structured assembly for tailored fusion materials.* Polym J, 2015. **47**(2): p. 89-98.
29. Fukuda, K., et al., *Exfoliated nanosheet crystallite of cesium tungstate with 2D pyrochlore structure: synthesis, characterization, and photochromic properties.* ACS Nano, 2008. **2**(8): p. 1689-95.
30. Schliehe, C., et al., *Ultrathin PbS sheets by two-dimensional oriented attachment.* Science, 2010. **329**(5991): p. 550-3.
31. Zhou, X., et al., *Atomic-Scale Spectroscopy of Gated Monolayer MoS2.* Nano Letters, 2016. **16**(5): p. 3148-3154.
32. Jin, W., et al., *Direct Measurement of the Thickness-Dependent Electronic Band Structure of ${\mathrm{MoS}}_{2}$ Using Angle-Resolved Photoemission Spectroscopy.* Physical Review Letters, 2013. **111**(10): p. 106801.
33. Brown, N.M.D., N. Cui, and A. McKinley, *An XPS study of the surface modification of natural MoS2 following treatment in an RF-oxygen plasma.* Applied Surface Science, 1998. **134**(1–4): p. 11-21.
34. Mas-Torrent, M. and C. Rovira, *Novel small molecules for organic field-effect transistors: towards processability and high performance.* Chemical Society Reviews, 2008. **37**(4): p. 827-838.
35. Lee, Y.H., et al., *Synthesis of large-area MoS2 atomic layers with chemical vapor deposition.* Adv Mater, 2012. **24**(17): p. 2320-5.
36. Xia, J., et al., *CVD synthesis of large-area, highly crystalline MoSe2 atomic layers on diverse substrates and application to photodetectors.* Nanoscale, 2014. **6**(15): p. 8949-55.
37. Shi, W., et al., *Synthesis design strategies to anisotropic chalcogenide nanostructures.* CrystEngComm, 2010. **12**(3): p. 641-659.
38. Yoshimoto, M., et al., *Atomic-scale formation of ultra-smooth surfaces on sapphire substrates for high-quality thin-film fabrication.* Appl Phys Lett, 1995. **67**.
39. Dumcenco, D., et al., *Large-Area Epitaxial Monolayer MoS2.* ACS Nano, 2015. **9**(4): p. 4611-4620.
40. Lee, C., et al., *Anomalous lattice vibrations of single- and few-layer MoS2.* ACS Nano, 2010. **4**(5): p. 2695-700.
41. Lembke, D. and A. Kis, *Breakdown of high-performance monolayer MoS2 transistors.* ACS Nano, 2012. **6**(11): p. 10070-5.
42. Liu, H. F. Wong, S. L. Chi, D. Z., *CVD Growth of MoS2-based Two-dimensional Materials.* Chemical Vapor Deposition, 2015. **21(**10-12): p.241-259.